Pergamon

Geochimica et Cosmochimica Acta, Vol. 68, No. 12, pp. 2725–2744, 2004

0016-7037/04 $30.00 + .00

doi:10.1016/j.gca.2003.11.024

Precise and accurate isotopic measurements using multiple-collector ICPMS

F. Albarède,[1,2,*] Philippe Telouk,[1] Janne Blichert-Toft,[1,2] Maud Boyet,[1] Arnaud Agranier,[2] and Bruce Nelson[1,3]

[1]Ecole Normale Supérieure de Lyon, 69007 Lyon, France
[2]California Institute of Technology, Pasadena, CA 91106, USA
[3]University of Washington, Seattle, WA 98195, USA

(*Received July* 3, 2003; *accepted in revised form November* 21, 2003)

Abstract—New techniques of isotopic measurements by a new generation of mass spectrometers equipped with an inductively-coupled-plasma source, a magnetic mass filter, and multiple collection (MC-ICPMS) are quickly developing. These techniques are valuable because of (1) the ability of ICP sources to ionize virtually every element in the periodic table, and (2) the large sample throughout. However, because of the complex trajectories of multiple ion beams produced in the plasma source whether from the same or different elements, the acquisition of precise and accurate isotopic data with this type of instrument still requires a good understanding of instrumental fractionation processes, both mass-dependent and mass-independent. Although physical processes responsible for the instrumental mass bias are still to be understood more fully, we here present a theoretical framework that allows for most of the analytical limitations to high precision and accuracy to be overcome. After a presentation of unifying phenomenological theory for mass-dependent fractionation in mass spectrometers, we show how this theory accounts for the techniques of standard bracketing and of isotopic normalization by a ratio of either the same or a different element, such as the use of Tl to correct mass bias on Pb. Accuracy is discussed with reference to the concept of cup efficiencies. Although these can be simply calibrated by analyzing standards, we derive a straightforward, very general method to calculate accurate isotopic ratios from dynamic measurements. In this study, we successfully applied the dynamic method to Nd and Pb as examples. We confirm that the assumption of identical mass bias for neighboring elements (notably Pb and Tl, and Yb and Lu) is both unnecessary and incorrect. We further discuss the dangers of straightforward standard-sample bracketing when chemical purification of the element to be analyzed is imperfect. Pooling runs to improve precision is acceptable provided the pooled measurements are shown to be part of a single population. Second-order corrections seem to be able to improve the precision on $^{143}Nd/^{144}Nd$ measurements. Finally, after discussing a number of potential pitfalls, such as the consequence of peak shape, correlations introduced by counting statistics, and the effect of memory on double-spike methods, we describe an optimal strategy for high-precision and accurate measurements by MC-ICPMS, which involves the repetitive calibration of cup efficiencies and rigorous assessment of mass bias combined with standard-sample bracketing. We suggest that, when these simple guidelines are followed, MC-ICPMS is capable of producing isotopic data precise and accurate to better than 15 ppm.

1. INTRODUCTION

Because of the intrinsic limitations of quadrupoles, mass spectrometers equipped with an inductively-coupled-plasma source were unable to produce precise isotopic measurements until they were fitted with a magnetic mass filter—which ensures flat top peaks—and multiple collection—which overcomes the instability of the plasma. Although the precision of the very first isotopic measurements by MC-ICPMS (Walder et al., 1993) remained somewhat unconvincing due to a combination of arduous issues, such as isobaric interferences, matrix effects, and the complex path of ions formed at very high temperatures, the techniques improved rapidly over the following years to the point where it could eventually be demonstrated that the typical between-run uncertainties of this particular analytical method were becoming very similar to the state-of-the-art of thermal ionization mass spectrometry (TIMS). In particular, routine external precision better than 0.35 epsilon units (35 ppm) can be achieved on Nd and Hf isotopic compositions (Blichert-Toft et al., 1997; Luais et al., 1997; Vance and Thirlwall, 2002). When this property is combined with the ability of the ICP source to ionize nearly all elements in the periodic system, thus producing precise isotopic compositions for poorly ionizing elements (Fe, Cu, Zr, Hf, W), and the possibility of correcting instrumental mass bias by the use of an element different from that being analyzed (e.g., Tl for Pb, Zn for Cu, and Yb for Lu) (Longerich et al., 1987, Rehkämper and Mezger, 1997; Belshaw et al., 1998; Maréchal et al., 1999; White et al., 2000; Blichert-Toft et al., 2002), the large sample throughput of MC-ICPMS gives this instrument a tremendous advantage over conventional TIMS. It is not exaggerating to assert that MC-ICPMS has now superseded TIMS for routine isotopic analysis of most elements and is the method of choice for the numerous elements that, for one reason or another, cannot be measured by TIMS.

The accuracy and precision of MC-ICPMS measurements are, however, still perceived as insufficiently validated, in particular with reference to TIMS. Dynamic measurements of Hf (Blichert-Toft et al., 1997) and Nd (Luais et al., 1997) isotope compositions have demonstrated that MC-ICPMS can produce accurate isotopic results, but this method remains tedious and inefficient for small samples. Consequently, essentially all MC-ICPMS instruments are run in static mode, which vividly exposes their major weakness: the transmission of an ion beam depends on both the trajectory and the collection device associated with each

* Author to whom correspondence should be addressed (albarede@ens-lyon.fr).

individual isotope to an extent that surpasses what is observed for TIMS measurements. Such strong isotopic bias, which will be discussed in more detail later in the paper, becomes increasingly severe as instruments get older and more contaminated by accumulating sample material. The isotopic bias is primarily due to the very high temperature of the plasma, which generates ions with different initial energies and therefore with complex trajectories in the mass spectrometer. The habit has been developed on some instruments to correct these effects by using "efficiencies" determined by calibration against known standard solutions. On the unwarranted assumption inherited from TIMS historical development that a good mass spectrometer should be able to yield accurate results without having to resort to complex data reduction, this correction is therefore often erroneously considered as a suspect "fudging" practice.

A new generation of TIMS is now commercially available for which ultra-high precision (typically less than 10 ppm) recently has been claimed, but mass fractionation behavior observed in that range of precision still remains a complex issue (Papanastassiou et al., 2003; Caro et al., 2003). In addition, given the immense success of the triple-spike method of isotopic measurements by TIMS in obtaining very precise Pb isotope data (Galer, 1999), this method is rapidly spreading to MC-ICPMS instruments (Thirlwall, 2002) and, inevitably, some discrepancies have appeared between these results and those obtained in static mode, especially when one element is used to correct the mass bias of another, such as in the case of Tl on Pb (Thirlwall, 2000, 2002). Finally, one downside to the large MC-ICPMS throughput is the capability of this instrument to generate large numbers of replicate analyses. By itself, this sheer number of data increases the number of seemingly inconsistent results that would only be occasionally produced with a more tedious and time-consuming technique.

The present study describes the theoretical foundations of the production of precise and accurate data by MC-ICPMS. Once these are established, we show how this theory accounts for the techniques of standard bracketing, and of isotopic normalization by a ratio of either the same or a different element. Accuracy is discussed with reference to the concept of efficiencies, and we also derive a general method to calculate more accurate ratios from dynamic measurements. We further discuss a number of potential pitfalls, such as the correlations introduced by counting statistics and the impact of memory effects on double-spike methods. A final discussion describes the pros and cons of each of the available approaches to high-precision and accurate measurements by MC-ICPMS.

A table of symbols and some analytical details relevant to the examples discussed in this article are given as Appendices.

2. A PHENOMENOLOGICAL DESCRIPTION OF THE MASS-DEPENDENT INSTRUMENTAL BIAS

Mass bias is mass fractionation introduced by the mass spectrometer. Although this topic has been covered before in a number of papers (Hofmann, 1971; Russell et al., 1978; Hart and Zindler, 1989; Habfast, 1998), the more general phenomenological theory of Maréchal et al. (1999) provides a unifying framework essential for the understanding of instrumental precision and will be briefly reviewed here.

Let us call N_k the number of atoms of the isotope k of an element of interest introduced into the mass spectrometer and n_k the number of charges forming the electronic signal of this isotope. Let us further call $\mathcal{T}(M_k)$ the transmission n_k/N_k of the isotope of mass M_k through the mass spectrometer. A variety of phenomena concur to create the condition for variable yield from one isotope to another even for a same element. Mass-dependent ionization, even at very high plasma temperatures, hydrodynamic entrainment by the expanding Ar atoms behind the cones (Niu and Houk, 1996), space-charge effects within the zone of electrical acceleration, and chromatic aberrations in the electrostatic sector, are all effects that may affect the transmission in a relatively smooth mass-dependent way.

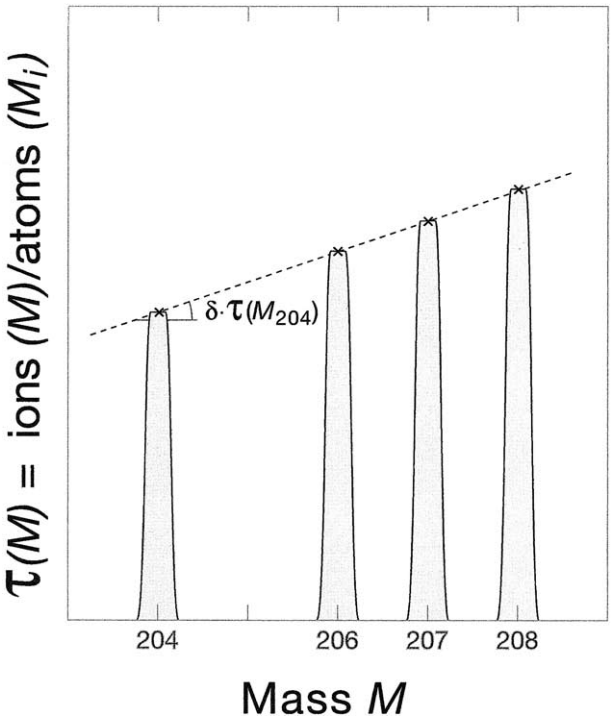

Fig. 1. Transmission as a function of the collector position along the focal plane. This position is parameterized by mass M. Transmission is the ratio between the number of ions of mass M_i arriving at the collector at mass M_i divided by the number of atoms of mass M_i introduced in the mass spectrometer. δ is the linear mass bias coefficient.

2.1. The Linear Law

This law (Fig. 1) is probably the most intuitive of all the mass-fractionation laws. Let us expand the transmission $\mathcal{T}(M)$ of isotopic beams at mass M as a function of the mass difference with a reference mass M_k:

$$\mathcal{T}(M) = \mathcal{T}(M_k) + \frac{\partial \mathcal{T}(M_k)}{\partial M}(M - M_k) + \mathbb{O}[(M - M_k)^2] \quad (1)$$

where $\mathbb{O}$ indicates that the remainder of the expansion is on the order of magnitude of the argument. Let us evaluate this expression for $M = M_i = M_k + \Delta M$ and divide the results by $\mathcal{T}(M_k)$:

$$\frac{\mathcal{T}(M_i)}{\mathcal{T}(M_k)} = 1 + \frac{\partial \ln \mathcal{T}(M_k)}{\partial M}(M_i - M_k) + O([M_i - M_k])^2 \quad (2)$$

Let us now call δ the derivative on the right-hand side evalu-

ated at $M = M_k$ and consider the first-order term only. The expression:

$$\frac{\mathcal{T}(M_i)}{\mathcal{T}(M_k)} \approx \frac{n_i/n_k}{N_i/N_k} \approx \frac{r_i}{R_i} \approx 1 + \delta(M_i - M_k) \quad (3)$$

gives the common form of the linear mass fractionation law. In this expression, r_i and R_i stand for the measured and true isotope ratios, respectively, with the implicit convention that the ratios have the reference isotope k at the denominator. The parameter δ is referred to as the linear mass bias. A typical mass bias for MC-ICPMS may vary from a few percent per amu at low mass to 1% per amu for high masses, such as Hf and Pb. This bias is typically an order of magnitude larger than for the characteristic bias incurred in TIMS measurements. Unfortunately, the linear law is not consistent: if two ratios fractionate according to the linear law, the ratio of these ratios does not.

2.2. The Power Law

Let us instead expand the logarithm of the transmission $\mathcal{T}(M)$ of isotopic beams at mass M as a function of the mass difference with a reference mass M_k:

$$\ln \mathcal{T}(M_k + \Delta M) = \ln \mathcal{T}(M_k) + \frac{\partial \ln \mathcal{T}(M_k)}{\partial M} \Delta M + \mathbb{O}(\Delta^2 M) \quad (4)$$

To the first order, the mass bias on the isotopic ratio N_i/N_k can be evaluated from:

$$\ln \mathcal{T}(M_i) - \ln \mathcal{T}(M_k) = \ln \frac{n_i/n_k}{N_i/N_k} \approx \delta(M_i - M_k) \quad (5)$$

We define the mass bias factor $g = e^{\delta}$ and finally obtain the expression for the so-called mass-fractionation power law as:

$$r_i \approx R_i g^{M_i - M_k} \quad (6)$$

2.3. The Exponential Law

The experimental law is evaluated similarly to the power law, but $\ln \mathcal{T}(M)$ is now expanded as a function of $\ln M$:

$$\ln \mathcal{T}(M_i) = \ln \mathcal{T}(M_k) + \frac{\partial \ln \mathcal{T}(M_k)}{\partial \ln M} (\ln M_i - \ln M_k) + \mathbb{O}([\ln M_i - \ln M_k]^2) \quad (7)$$

To the first order, the mass bias on the isotopic ratio N_i/N_k is evaluated from:

$$\ln \mathcal{T}(M_i) - \ln \mathcal{T}(M_k) = \ln \frac{n_i/n_k}{N_i/N_k} \approx \frac{\partial \ln \mathcal{T}(M_k)}{\partial \ln M} \ln \frac{M_i}{M_k} \quad (8)$$

The mass bias factor β is defined as:

$$\beta = \frac{\partial \ln \mathcal{T}(M_k)}{\partial \ln M} = M_k \delta \quad (9)$$

from which we get the mass-fractionation exponential as:

$$r_i \approx R_i \left(\frac{M_i}{M_k}\right)^{\beta} \quad (10)$$

2.4. The Generalized Power Law

Maréchal et al. (1999) showed that the exponential and the power laws are special cases of a more general mass-fractionation law. This general law is obtained by expanding $\ln \mathcal{T}(M)$ as a function of M^q, where q is an arbitrary exponent:

$$\ln \mathcal{T}(M_i) - \ln \mathcal{T}(M_k) = \ln \frac{n_i/n_k}{N_i/N_k} \approx \frac{\partial \ln \mathcal{T}(M_k)}{\partial M^q} (M_i^q - M_k^q) \quad (11)$$

Defining the fractionation coefficient h as:

$$\ln h = \frac{\partial \ln \mathcal{T}(M_k)}{\partial M^q} \quad (12)$$

Maréchal et al. (1999) obtained the general result:

$$r_i \approx R_i h^{M_i^q - M_k^q} \quad (13)$$

and defined the fractionation factor $f = q \ln h$. The power law is obtained for $q = 1$. The exponential law is obtained as a limit for $q \to 0$ (Maréchal et al., 1999) and then $f = \beta$. Other laws are easily obtained, such as the law resulting from the distribution of atom energy over vibrational quantum levels with $q = -1$ (e.g., Criss, 1999). Kehm et al. (2003) suggest an alternative mass-fractionation law:

$$r_i \approx R_i \mathcal{H}^{\int_{M_k}^{M_i} M^n dM} \quad (14)$$

where $\mathcal{H}$ is the mass-fractionation parameter and n is an arbitrary exponent. The sum in the exponent can be exactly integrated, which gives:

$$r_i \approx R_i \mathcal{H}^{\frac{M_i^{n+1} - M_k^{n+1}}{n+1}} \quad (15)$$

Replacing $n + 1$ by q and $\mathcal{H}$ by h^q demonstrates that the mass-fractionation law of Kehm et al. (2003) is identical to the generalized power law of Maréchal et al. (1999).

A first property of the generalized power law and its power and exponential special cases is that ratios of ratios follow consistent mass-fractionation laws: if both $^{206}Pb/^{204}Pb$ and $^{207}Pb/^{204}Pb$ fractionate according to the generalized power law, so does their ratio $^{207}Pb/^{206}Pb$.

The second remarkable property of the generalized power law is that linear alignments are obtained in log-log plots, in which one measured isotopic ratio is plotted against another, thereby reducing the need to determine which value of q and therefore which particular mass fractionation law holds for the measurements. Provided run conditions are left unchanged between two runs of the same sample solution, the relationships between the isotopic proportions of the two runs are simply related. In a log-log plot, several runs of a same known solution for various values of the mass-bias function h must form an alignment with the slope $M_i^q - M_k^q$ (Fig. 2). Taking the logarithm of Eqn. 13 for two ratios i/k and j/k, we obtain:

$$\frac{\ln r_i - \ln R_i}{\ln r_j - \ln R_j} = \frac{M_i^q - M_k^q}{M_j^q - M_k^q} = s_{j/k}^{i/k} \quad (16)$$

For example, we obtain the expression of the slope $s_{206/204}^{207/204}$ of

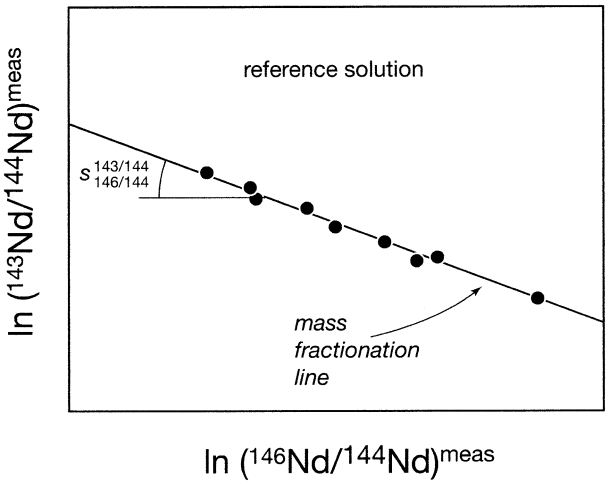

Fig. 2. Plot of ln (^{143}Nd/^{144}Nd)^{meas} vs. ln (^{146}Nd/^{144}Nd)^{meas} of a Nd solution run several times within a short time interval. $s^{143/144}_{146/144}$ is the slope $(M^q_{143} - M^q_{144})/(M^q_{146} - M^q_{144}) \approx -0.5$ of the alignment. The position of a given measurement along the mass fractionation line is a relative measure of the mass bias and does not evolve steadily through time.

the alignment of Pb isotopic ratios of a same lead solution in the plot of log ^{207}Pb/^{204}Pb vs. log ^{206}Pb/^{204}Pb as:

$$s^{207/204}_{206/204} = \frac{M^q_{207Pb} - M^q_{204Pb}}{M^q_{206Pb} - M^q_{204Pb}} \tag{17}$$

with the limit solution for the exponential law:

$$s^{207/204}_{206/204} = \frac{\ln (M_{207Pb}/M_{204Pb})}{\ln (M_{206Pb}/M_{204Pb})} \tag{18}$$

For mixed solutions of two elements, such as Zn and Cu, or Pb and Tl, this linear property still holds provided their two fractionation factors f are proportional (Fig. 3). For Pb and Tl and an exponential law ($f = \beta$), we can write the slope of the mass-fractionation line in an ln ^{207}Pb/^{204}Pb vs. ln ^{205}Tl/^{203}Tl diagram as:

$$s^{207/204}_{205/203} = \frac{\beta^{Pb}}{\beta^{Tl}} \frac{\ln (M_{207Pb}/M_{204Pb})}{\ln (M_{205Tl}/M_{203Tl})} \tag{19}$$

We will see that, in principle, there is no need to determine the actual value of q for a given series of runs, but should the "true" isotopic composition of a sample be known (e.g., for gravimetrically prepared standards) or estimated from TIMS measurements under conditions of well-controlled mass bias, the value of q can be determined for the conditions at which the MC-ICPMS is operated. In this way, Maréchal et al. (1999) deduced from a series of Zn isotope measurements that the exponential law accounts for the patterns of the Zn mass bias on the Lyon Plasma 54.

A third property of the generalized power law is the mass fractionation $(\Delta R/R)_1$ per mass unit difference for constant h at a given q:

$$\left(\frac{\Delta R}{R}\right)_1 = \frac{1}{M_i - M_k}\left(\frac{r_i}{R_i} - 1\right) \tag{20}$$

Expressions for $(\Delta R/R)_1$ have been tabulated for q in the range $[-2, +2]$ by Maréchal et al. (1999). For the power law ($q = 1$), mass fractionation is constant across the mass range, while it varies as M^{-1} for the exponential law ($q = 0$). Blichert-Toft et al. (1997) used this particular feature to establish that the exponential law is best suited for the Lyon MC-ICPMS.

For small extents of isotopic fractionation, the generalized power law, and therefore also the other laws considered above, reduces to the *linear law* and the linear fractionation coefficient δ is easily shown to converge towards $M_k^{q-1} f$.

3. STANDARD BRACKETING METHODS

In a variety of techniques, notably gas-source mass spectrometry, standard bracketing methods have been used for

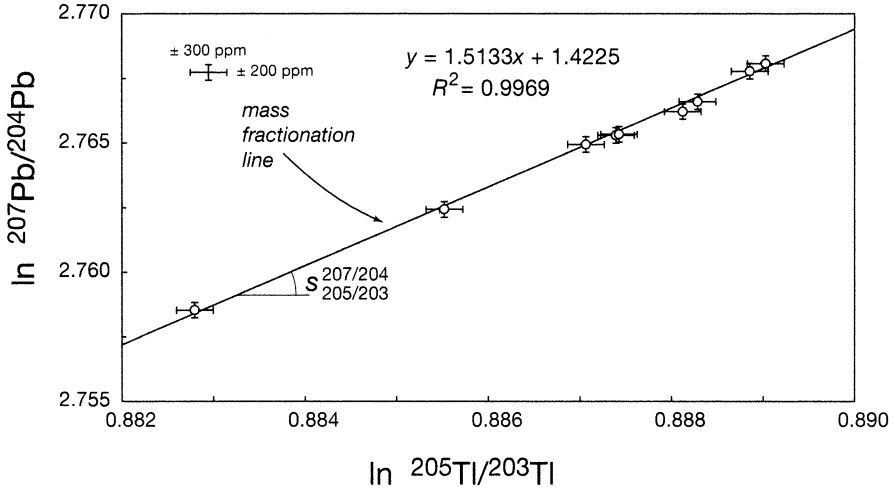

Fig. 3. Plot of ln (^{207}Pb/^{204}Pb)^{meas} vs. ln (^{205}Tl/^{203}Tl)^{meas} of a mixed Pb-Tl solution run several times between samples over a period of 12 h. The linear relation holds even when the elements appearing on each axis are different. Although the slope $s^{207/204}_{205/203}$ of the alignment (1.513) is similar to the value predicted from the mass relationship (1.489) of the exponential, such a difference may change the corrected ^{207}Pb/^{204}Pb ratio by almost 400 ppm.

decades to interpolate the mass bias of an unknown sample between the biases inferred from two standard runs, one preceding and one following the sample analysis (less stringent orders of interpolation are also used). Let us divide Eqn. 10 for the sample by the same equation for a standard (std1) run just before the sample. We get:

$$\frac{(R_i)_{\text{sple}}}{(R_i)_{\text{std}}} = \frac{(r_i)_{\text{sple}}}{(r_k)_{\text{std1}}} \left(\frac{M_i}{M_k}\right)^{\beta_{\text{std1}}-\beta_{\text{sple}}} \tag{21}$$

with a similar equation for the standard (std2) run just after the sample. We now assume that

$$\beta_{sple} = (1-\theta)\beta^1_{\text{std}} + \theta\beta^2_{\text{std}} \tag{22}$$

in which θ is a constant analogous to a time and chosen between 0 and 1. We now get

$$\frac{(R_i)_{\text{sple}}}{(R_i)_{\text{std}}} = \frac{(r_i)_{\text{sple}}}{(r_i)_{\text{std1}}} \left(\frac{M_i}{M_k}\right)^{\theta(\beta_{\text{std1}}-\beta_{\text{std2}})} \tag{23}$$

$$\frac{(R_i)_{\text{sple}}}{(R_i)_{\text{std}}} = \frac{(r_i)_{\text{sple}}}{(r_i)_{\text{std2}}} \left(\frac{M_i}{M_k}\right)^{(1-\theta)(\beta_{\text{std2}}-\beta_{\text{std1}})} \tag{24}$$

Raising the first of these equations to the power of $1-\theta$ and the second to the power of θ and then multiplying them, the terms in M_i/M_k cancel out and we obtain:

$$(R_i)_{\text{sple}} = (R_i)_{\text{std}} \frac{(r_i)_{\text{sple}}}{(r_i)^{1-\theta}_{\text{std1}} \times (r_i)^{\theta}_{\text{std2}}} \tag{25}$$

This interpolation scheme requires a choice of the value of θ, which is commonly chosen to be equal to 0.5 (mid-point) whenever samples and standards alternate regularly. This is a fairly general approach, which amounts to linearly interpolating the logarithms of the isotopic ratios.

Equation 22 shows that mass fractionation by simple interpolation between standards, i.e., without internal or external isotopic normalization, is correct only when mass fractionation changes smoothly upon alternating between standards and samples, which requires extremely strict sample purification. A heavy sample matrix (typically more concentrated than the element being analyzed) significantly changes fractionation (e.g., Woodhead, 2002). The presence of sample matrix often results in β_{sple} falling outside the range $[\beta^1_{\text{std}} - \beta^2_{\text{std}}]$ and thus nullifies the basic assumption of the method.

4. IMPLEMENTATION OF THE FIRST-ORDER MASS BIAS CORRECTION

As shown by Maréchal et al. (1999) and White et al. (2000), the linearity property of the isotopic array formed in log-log plots by all the measurements of a same solution can be used to obtain the isotopic ratio of a sample with respect to the same ratio in a standard solution of known isotopic properties. Taking the logarithm of Eqn. 13 for both the sample and the standard and dividing this equation by the same equation for the ratio N_j/N_k, we obtain:

$$\frac{\ln(R_i)_{\text{sple}} - \ln(r_i)_{\text{sple}}}{\ln(R_j)_{\text{sple}} - \ln(r_j)_{\text{sple}}} = \frac{\ln(R_i)_{\text{std}} - \ln(r_i)_{\text{std}}}{\ln(R_j)_{\text{std}} - \ln(r_j)_{\text{std}}} = \frac{M^q_i - M^q_k}{M^q_j - M^q_k} = s^{i/k}_{j/k} \tag{26}$$

in which the slope $s^{i/k}_{j/k}$ can be calculated either from the fractionation law that best describes the mass spectrometer used by the analyst or determined by running standard solutions. We will assume that the uncertainty on the slope does not induce a significant error on the corrected ratios. Let us define the intercept I_{sple} of the mass fractionation line with the y-axis as:

$$I_{\text{sple}} = r_i - s^{i/k}_{j/k} r_j \tag{27}$$

We can rearrange Eqn. 26 as:

$$\ln(R_i)_{\text{sple}} = s^{i/k}_{j/k} \ln(R_j)_{\text{sple}} + I_{\text{sple}} \tag{28}$$

with a similar equation for the standard. This equation provides an analytic formulation of the principles developed by Maréchal et al. (1999). These mass fractionation equations can be used to solve two common types of problems. First, as for Sr, Nd, and Hf, a common reference R_j is chosen for internal normalization (e.g., $^{146}Nd/^{144}Nd = 0.7219$). This amounts to removing all the mass-dependent fractionation effects (both natural and analytical) so as to preserve only radiogenic, cosmogenic, and/or nucleosynthetic isotopic deviations, and to assuming that R_j is constant. By subtracting Eqn. 28 for the sample from the same equation for the standard, we get the key expression:

$$\ln(R_i)_{\text{sple}} = \ln(R_i)_{\text{std}} + I_{\text{sple}} - I_{\text{std}} \tag{29}$$

For Nd, for example, we would get

$$\ln(^{143}Nd/^{144}Nd)^{\text{corr}}_{\text{sple}} = \ln(^{143}Nd/^{144}Nd)^{\text{true}}_{\text{std}} + I_{\text{sple}} - I_{\text{std}} \tag{30}$$

in which the "true" (accepted) value of the standard stands for the corrected value. I defined as

$$I = \ln(^{143}Nd/^{144}Nd)^{\text{meas}} - s^{143/144}_{146/144} \ln(^{146}Nd/^{144}Nd)^{\text{meas}} \tag{31}$$

is the intercept of the straight line with slope $s^{143/144}_{146/144}$ drawn through the point with coordinates $x = \ln(^{146}Nd/^{144}Nd)^{\text{meas}}$ and $y = \ln(^{143}Nd/^{144}Nd)^{\text{meas}}$. A different choice of normalization ratio would give the same result. The difference between the logarithm of the mass-bias corrected ratios for the sample and the standard is simply the vertical distance between the parallel lines with a slope of $s^{143/144}_{146/144}$ drawn through the points representing the sample and the standard. The slope $s^{143/144}_{146/144}$ does not even have to be determined from the same solution as the standard (Fig. 4). To avoid amplification of the uncertainty on $s^{143/144}_{146/144}$ and thereby to achieve high accuracy, it is essential that the abscissas of the two runs $(^{146}Nd/^{144}Nd)^{\text{meas}}$ are as similar to each other as possible and therefore that the materials to be analyzed are extremely well purified. To a good approximation and regardless of the reference material (chon-

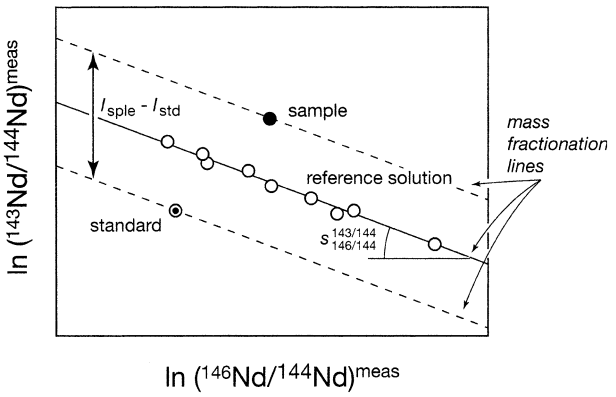

Fig. 4. Principle of the mass bias correction for a Nd sample. The slope $s^{143/144}_{146/144}$ is determined by measuring any Nd shelf solution suitable as a reference (open circles), preferably, but not necessarily, a standard solution. The difference between a particular sample and a standard is equal to the vertical distance between the lines drawn through the points representing the sample and the standard and with a slope equal to $s^{143/144}_{146/144}$.

drites or other), Eqn. 30 relates the difference $\Delta I = I_{sple} - I_{std}$ to the difference in $\Delta\varepsilon = \varepsilon_{sple} - \varepsilon_{std}$ through:

$$\Delta\varepsilon \approx 10{,}000\Delta I \tag{32}$$

A second situation arises when there is no stable ratio that can be used as reference, which is the case for Pb, but also for elements with only two isotopes (Cu, Rb, Lu). It may also be that it is the mass-dependent isotopic fractionation itself that is sought, e.g., for the stable isotope geochemistry of Zn, Fe, Ge, and many other such elements. It is noteworthy that the previous equations do not require that the isotopic ratio used for normalization (*x*-axis) and the ratio to be established (*y*-axis) have to be for the same element. The original formulation of this property by Longerich et al. (1987) assumed identical isotopic fractionation factors for the two elements, but this is not at all a necessary constraint and we will show below that, in fact, the use of this very assumption may lead to significant error. Let us consider a mixed Pb-Tl solution. Let us define $s^{206/204}_{205/203}$ as the slope of the isotopic analyses of standard solution alignment in a plot of $y = \ln {}^{206}Pb/{}^{204}Pb$ vs. $x = \ln {}^{205}Tl/{}^{203}Tl$. The condition necessary for this array to be linear is that $(\beta^{Pb}/\beta^{Tl})_{sple} = (\beta^{Pb}/\beta^{Tl})_{std}$, which is yet another call for near-perfect Pb purification. For a same value of the normalizing $^{205}Tl/^{203}Tl$ ratio in the mixed standard solution and in the sample doped with a Tl spike solution, a form similar to Eqn. 29 can be written:

$$\ln ({}^{206}Pb/{}^{204}Pb)^{corr}_{sple} = \ln ({}^{206}Pb/{}^{204}Pb)^{true}_{std} + I_{sple} - I_{std} \tag{33}$$

where:

$$I = \ln ({}^{206}Pb/{}^{204}Pb)^{meas} - s^{206/204}_{205/203} \ln ({}^{205}Tl/{}^{203}Tl)^{meas} \tag{34}$$

For Pb, Cu, or Zn, the raw values of the standard used as a reference to define the reference mass fractionation line (primary standard) should not be used for inter-laboratory comparisons. For Pb, the lack of secondary standards with isotopic compositions reasonably close to the composition of the NIST 981 standard is a serious limitation to the cross-calibration of the relative precision of different instruments.

The slope $s^{i/k}_{j/k}$ is best estimated from the isotopic ln r_i vs. ln r_j array for a shelf solution and should be carefully determined for the interval during which the samples are measured. Standards bracketing the measured samples do not provide the best estimate of this slope: their isotope compositions are either very similar, in which case the error on the slope is large, or very different, which usually reflects a heavy matrix in the intercalated sample solution that abruptly changed the mass bias over an unknown period of time. Provided the alignment is good, we therefore rather suggest to use the slope determined on a large set of standards run over a period of several hours in alternation with samples. Woodhead (2002) suggests to use reference solutions doped with elements similar to those present in the sample matrix. A less rigorous method is to assume that the value of q is known, which may be true for a certain type of mass spectrometers: on the Plasma 54 in Lyon, q could never be shown to deviate significantly from 0 (exponential law). A precise knowledge of the exponent q is, however, never a prerequisite for obtaining precise measurements, although q must be known for accurate results to be achieved.

The implicit assumption in this correction is that both of the mass fractionation factors h, e.g., for Pb and Tl, or Cu and Zn, are different, but that their ratio remains constant upon switching between sample and standard solutions. Again, this assumption stands better chances of being correct if purification of the sample has been efficient. For Cu, Zn, and the Pb isotope ratios that are the closest to unity ($^{207}Pb/^{206}Pb$ and $^{208}Pb/^{206}Pb$), a precision of 50 ppm can be achieved (Maréchal et al., 1999; White et al., 2000). For larger ratios, such as $^{206}Pb/^{204}Pb$ and $^{207}Pb/^{204}Pb$, the obtainable precision is 200–400 ppm.

An important application of this theory is the precise correction of both isobaric interferences and mass bias for isotope dilution. Its application to the isotope dilution of Lu in the presence of Yb is described in Blichert-Toft et al. (2002) and Barfod et al. (2003). On the one hand, the presence of Yb in the Lu fraction creates an interference on mass 176, which, in principle, is a disadvantage, but Yb-Lu separation is excruciatingly difficult. On the other hand, the presence of Yb together with Lu can also be considered an advantage in that it allows the analyst to control the instrumental mass bias. From the preceding discussion, it is understood that, once normalization to a "clean" isotope ratio has been made, the difference in the other isotopic ratios needs no further correction for mass bias. Let us thus write that Lu and Yb overlap at mass 176, whereas Yb is interference-free at mass 171 and Lu is interference-free at mass 175 and note T as the total signal at a given mass:

$$\frac{^{176}Lu}{^{175}Lu} = \frac{^{176}Lu}{^{176}T}\frac{^{176}T}{^{175}Lu} = \left(1 - \frac{^{176}Yb}{^{176}T}\right)\frac{^{176}T}{^{175}Lu} = \left[1 - \frac{(^{176}Yb/^{171}Yb)_{Yb\ std}}{(^{176}T/^{171}T)_{Lu+Yb\ mix}}\right]\frac{^{176}T}{^{175}T} \tag{35}$$

When this expression evaluated for a run of a spiked sample is divided by the same expression for an Yb + Lu standard

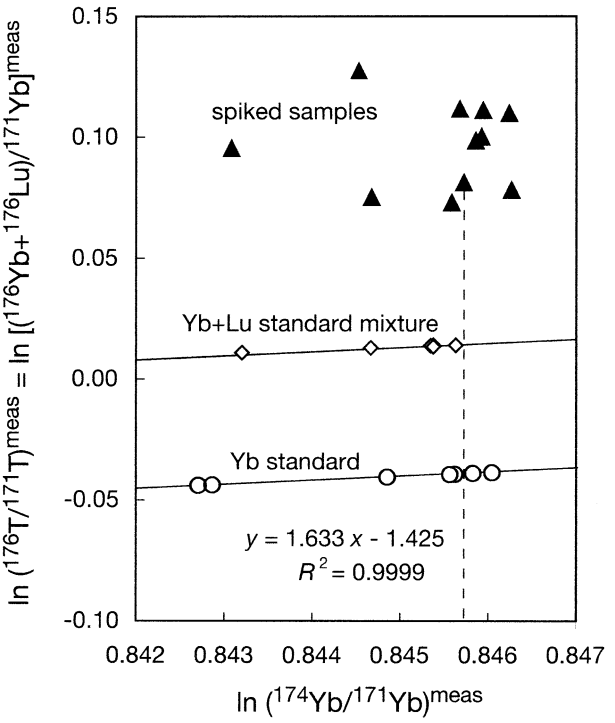

Fig. 5. Principle of isotope dilution when both isobaric interferences and instrumental mass bias are present. A position along the horizontal axis (dashed vertical line) corresponds to a unique value of the mass bias. Solutions of pure Yb standard and mixed Yb-Lu standards are run in between the spiked samples. Their slope is consistent with the theoretical slope inferred from mass differences (≈5/3). The straight lines obtained on the standards can be interpolated at the sample value of $^{174}Yb/^{171}Yb$. At this stage, comparison between the ordinates of the sample and the interpolated Yb-Lu mixture gives the $^{176}Lu/^{175}Lu$ of the spiked sample and therefore its Lu concentration.

mixture, it is possible to obtain the $^{176}Lu/^{175}Lu$ of the spiked sample and thereby derive its concentration by the standard equations of isotope dilution. The only requirement is that all the ratios must be evaluated for a same extent of mass fractionation. This is conveniently achieved by interpolating in Fig. 5 the mass fractionation lines of the standard solutions at the value of $^{174}Yb/^{171}Yb$ of the sample run. This, of course, cannot be rigorously done for the isotopic composition of the pure spike solution, but unless the sample is severely overspiked, the incidence on errors from assuming that mass fractionation in the spike run is similar to the average fractionation of a standard solution, is negligible. Despite the low abundance of ^{176}Lu, this technique allows for the routine precision of 0.2–0.5 per mil to be obtained for Lu/Hf ratios (as precise hafnium concentrations are readily obtained on pure Hf fractions by isotope dilution with internal correction of the mass bias).

5. IMPLEMENTATION OF THE SECOND-ORDER MASS BIAS CORRECTION

Let us first describe an exact, single stage of second-order correction, which will be evaluated here for the exponential law. Retaining the second-order term of Eqn. 7 and 9, we obtain:

$$\ln \mathcal{T}(M_i) = \ln \mathcal{T}(M_k) + \beta' \ln \frac{M_i}{M_k} + \frac{\gamma}{2} \ln^2 \frac{M_i}{M_k} + \mathcal{O}\left(\ln^3 \frac{M_i}{M_k} \right) \tag{36}$$

where β' and γ are the first- and second-order coefficients, respectively, of the $\ln \mathcal{T}$ expansion with respect to M in the neighborhood of M_k. From the way it is evaluated, the first-order coefficient β' of the second-order expansion is different from the equivalent coefficient β in the first-order expansion. Using μ_i for $\ln (M_i/M_k)$, this equation can be simplified as:

$$\ln \frac{r_i}{R_i} \approx \beta' \mu_i + \gamma \frac{\mu_i^2}{2} \tag{37}$$

Two normalization ratios R_i and R_j are required to solve this equation in β' and γ, and the solution is:

$$\beta' = \frac{\mu_j}{\mu_i(\mu_j - \mu_i)} \ln \frac{r_i}{R_i} - \frac{\mu_i}{\mu_j(\mu_j - \mu_i)} \ln \frac{r_j}{R_j} = \frac{\mu_j \beta_i - \mu_i \beta_j}{\mu_j - \mu_i}$$
$$\gamma = -\frac{2}{\mu_i(\mu_j - \mu_i)} \ln \frac{r_i}{R_i} + \frac{2}{\mu_j(\mu_j - \mu_i)} \ln \frac{r_j}{R_j} = 2 \frac{\beta_j - \beta_i}{\mu_j - \mu_i} \tag{38}$$

where β_i and β_j are calculated using the standard first-order exponential law for the ratios r_i and r_j. The last expression of γ indicates that a second-order correction is appropriate whenever the first-order β_i values vary linearly with the mass difference.

A two-stage technique aimed at handling the second-order effects was proposed by Thirlwall (1991) and subsequently used by Vance and Thirlwall (2002) and Caro et al. (2003) for Nd isotope analysis. These authors opted for two successive steps of correction. In each case, the first step of correction uses an exponential law with normalization to $^{146}Nd/^{144}Nd = 0.7219$. Thirlwall (1991) and Vance and Thirlwall (2002) used the correlation between the first-step corrected ratios of standard solutions to normalize $^{143}Nd/^{144}Nd$ to a fixed value of $^{142}Nd/^{144}Nd$ and succeeded in reducing the variance of their measurements. Caro et al. (2003) used the same procedure to refine the exponential correction of $^{143}Nd/^{144}Nd$ and $^{142}Nd/^{144}Nd$ by assuming a constant $^{150}Nd/^{144}Nd$. Figure 6 shows the topology of this correction in three dimensions. We will now show that a second-order correction can be implemented without an a priori determination of a fractionation line on standard solutions.

Two normalization ratios $R_i(^{146}Nd/^{144}Nd)$ and $R_j(^{142}Nd/^{144}Nd)$ are used to correct the bias on an unknown ratio R_x ($^{143}Nd/^{144}Nd$). After the first step of exponential correction (Eqn. 10), the measured ratio r_j becomes r_j^e with:

$$\ln \frac{r_j}{r_j^e} = \beta \mu_j = \frac{\mu_j}{\mu_i} \ln \frac{r_i}{R_i} \tag{39}$$

Using Eqn. 37, this equation is rewritten as:

$$\ln \frac{r_j}{r_j^e} = \mu_j \left(\beta' + \frac{\gamma}{2} \mu_i \right) \tag{40}$$

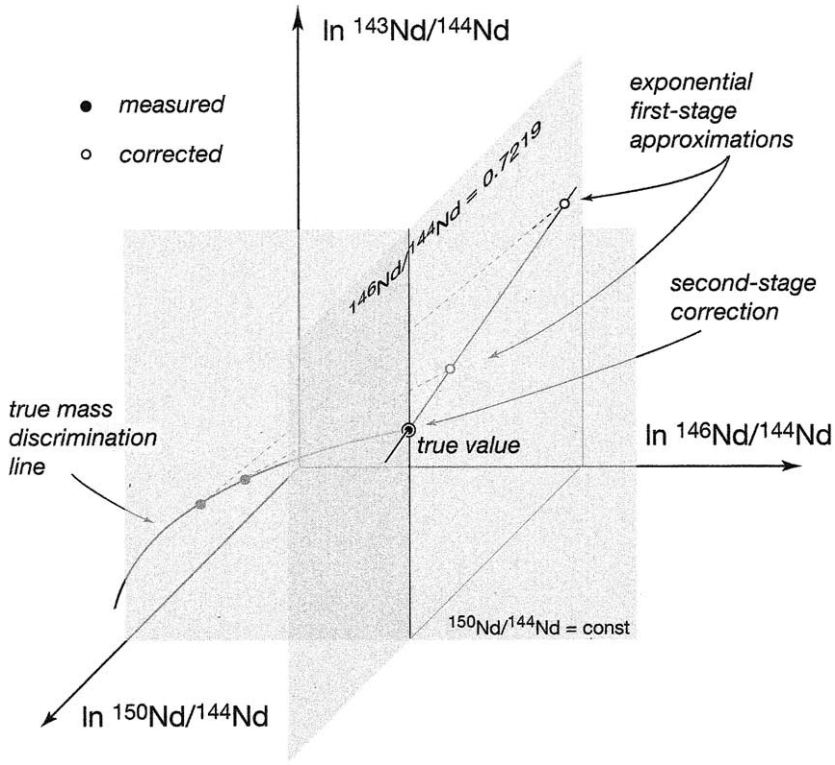

Fig. 6. Topology of Thirlwall's (1991) two-stage correction using the $^{150}Nd/^{144}Nd$ ratio as a second reference. The same standard solution is analyzed several times and the data are first corrected to $^{146}Nd/^{144}Nd = 0.7219$ using an exponential law. The points corrected after the first stage form an alignment in a $^{143}Nd/^{144}Nd$ vs. $^{150}Nd/^{144}Nd$ plot and can now be corrected to a reference value of $^{150}Nd/^{144}Nd$. It is assumed that the slope of the $^{143}Nd/^{144}Nd$ vs $^{150}Nd/^{144}Nd$ correlation is the same regardless of the sample and that the second-stage correction is small.

and a similar expression holds for r_x^e. Moreover, Eqn. 37 for R_j reads:

$$\ln \frac{r_j}{R_j} = \mu_j \left(\beta' + \frac{\gamma}{2} \mu_j \right) \tag{41}$$

Dividing the last two equations by μ_j and subtracting them gives:

$$\ln \frac{r_j^e}{R_j} = \frac{\gamma}{2} \mu_j (\mu_j - \mu_i) \tag{42}$$

Writing a similar expression for R_x shows that the exponentially corrected ratios r_j^e and r_x^e are correlated and that the correlation line goes through the values of the "true" R_j and R_x ratios. The correction expression is:

$$R_x = r_x^e \left(\frac{R_j}{r_j^e} \right)^{\frac{\mu_x}{\mu_j} \frac{\mu_x - \mu_i}{\mu_j - \mu_i}} \tag{43}$$

An application of this correction scheme will be presented below. In the cases considered by Thirlwall (1991) and Vance and Thirlwall (2002), the slope of the correlation between the exponentially corrected values of $^{143}Nd/^{144}Nd$ and $^{142}Nd/^{144}Nd$ is ≈ 0.2, which agrees with the predictions of this theory.

Regardless of the success of the two-stage scheme, utmost care must be exercised in validating such a gain of precision: a two-stage correction based on the residuals of a single-stage correction *must* improve the apparent precision regardless of the underlying physics of mass fractionation. Such an improvement is a straightforward statistical effect, which simply reflects that two free parameters always provide a better fit than one. Checking that the slope between the exponentially corrected values fits the predicted value is a good test of whether a second-order correction is appropriate.

6. MASS-INDEPENDENT FRACTIONATION

Mass fractionation can be viewed as a combination of mass-dependent and mass-independent effects. The former is what has been dealt with so far and largely results from a spread in the ion energy during ionization and transport in the mass spectrometer. The latter can be viewed as a scatter of the actual transmission around the dashed straight line shown in Figure 1. Mass-independent biases arise as a consequence of a number of problems, of which the most important are: (1) a sloping or rounded peak top may result from the imperfect z-focusing of the ion beams; (2) the ion beams may have cross sections so broad that they become partially clipped along their trajectory in the flight tube, especially for off-axis masses; (3) secondary electrons may not be suppressed with a 100% efficiency; (4) scattered ions of various masses may bounce around the collection system and be picked up by the wrong detector; (5) collisions of ions in the flight tube behind the magnet produce some energy scatter which results in a continuous background affecting the true zero value; (6) the response of

resistors may be nonlinear; and (7) counting statistics (see below). Although these problems usually involve only a very small fraction of the ion current (typically less than 500 ppm) for modern mass spectrometers, they may nevertheless alter the precision of the measurements in a way that is not a linear function of the mass difference between the beams collected in the Faraday cups. In addiition, 500 ppm is significant when aiming at <100 ppm precision for isotopic measurements.

Let us illustrate the mass-independent fractionation issue with the case of an imperfectly flat peak top: transmission at a given mass changes with detector position independently of the mass to be collected. Peak tops may be round, sloping, or both. These imperfections will strongly affect the isotopic ratios. For Sr and Nd, Thirlwall (1991) noted that, even after mass-fractionation correction, a truncated peak could leave spuriously correlated ratios, but asserted that a sloping peak should have no effect. The effect of peak shape is therefore a fairly general problem. Let us call $M = M_i + \delta M_i$ the actual position of the cup with respect to its ideal position at mass M_i. The measured ratio must now be expanded as a function of mass *and* cup position. Assuming for the sake of illustration that the mass fractionation law is exponential and that the peak top is sloping, a first-order expansion is sufficient. We obtain:

$$r_i \approx R_i\left(\frac{M_i + \delta M_i}{M_k + \delta M_k}\right)^{\beta} \approx R_i\left(\frac{M_i}{M_k}\right)^{\beta}\left(\frac{1 + \delta M_i/M_i}{1 + \delta M_k/M_k}\right)^{\beta} \quad (44)$$

and the exponentially corrected ratio as:

$$r_i^e = R_i\left(\frac{1 + \delta M_i/M_i}{1 + \delta M_k/M_k}\right)^{\beta} \quad (45)$$

A deviation from the ideal first-order fractionation law will appear as a residual correlation between the ratios corrected for mass bias using the exponential law. It can be verified that even very small $\delta M/M$ in Eqn. 45 produces a potentially important isotopic effect on the order of $1 + \beta(\delta M_i - \delta M_k)/M_k$. The alignment of the correlation between the corrected ratios $x = \ln r_i^e$ and $y = \ln r_j^e$ produced by sloping peaks in a log-log plot has a slope of $\approx \delta M_j/\delta M_i$. For a round peak, a second-order term should be included.

If the isotopic composition of a standard solution of the element under consideration is known, at least for an adopted value of a reference ratio, such as $^{146}Nd/^{144}Nd = 0.7219$, mass-independent isotopic fractionation can be conveniently dealt with by introducing correction factors (also known as efficiencies), which are determined by measuring the standard and comparing its isotopic abundances with the known values. Let us first demonstrate, however, that although these mass-independent effects change the measured isotopic compositions, they do so in a way that preserves the slope of the linear alignments in log-log plots and therefore allows isotopic variations among standards to be determined with an excellent precision.

Let the transmission $\mathcal{T}_k^{\gamma}$ at mass k in collector γ be the product of a mass-dependent bias $\mathcal{Y}(M_k)$ and a cup-dependent factor (efficiency) $\mathcal{A}_{\gamma}$

$$n_k/N_k = \mathcal{A}_{\gamma}\mathcal{Y}(M_k) \quad (46)$$

The symbol $\mathcal{Y}(M_k)$ represents the mass bias when all the masses are peak-jumped in the same cup, such as done by the standard procedure still employed on all single-collector mass spectrometers. If we assume that mass i is collected in cup α and the bias $\mathcal{Y}(M)$ follows the generalized power-law with exponent q, we obtain the expression for the measured ratio of masses i to k as

$$r_i = \frac{\mathcal{A}_{\alpha}}{\mathcal{A}_{\gamma}} R_i h^{M_i^q - M_k^q} \quad (47)$$

Writing a similar equation for the ratio N_j/N_k with the assumption that mass j is collected in cup β, we can write

$$\frac{\ln R_j - \ln r_j - \ln \mathcal{A}_{\beta}/\mathcal{A}_{\gamma}}{\ln R_i - \ln r_i - \ln \mathcal{A}_{\alpha}/\mathcal{A}_{\gamma}} = \frac{M_j^q - M_k^q}{M_i^q - M_k^q} = s_{i/k}^{j/k} \quad (48)$$

In other words, variable cup efficiencies change the intercept, not the slope, of the mass-fractionation curves, and the procedure for correcting mass fractionation with respect to a standard is similar to the case in which no cup efficiencies are involved.

7. CORRECTION OF THE INSTRUMENTAL BIAS IN DYNAMIC MODE

Mass-independent isotopic fractionation is most often corrected for by running the samples in dynamic mode, i.e., by switching the electromagnetic field and therefore the masses across the cups, thus allowing the efficiencies to cancel out between different beam configurations (Dodson, 1963; Ludwig, 1997; Wendt and Haase, 1998). Luais et al. (1997) and Blichert-Toft et al. (1997) published solutions for the dynamic analyses of $^{143}Nd/^{144}Nd$ and $^{176}Hf/^{177}Hf$, respectively, using an exponential law for mass bias, but these solutions are rather cumbersome. Similarly, Wendt and Haase (1998) presented a solution to the problem of dynamic analysis with cup efficiencies, but again the calculations are fairly heavy to implement. An apparently simple method consists in evaluating cup factors by simply commuting isotopic beams with the same mass difference into the same pair of cups and comparing their ratios, one of which is assumed to be known, e.g., $^{208}Pb/^{206}Pb$, as in Thirlwall (2000). Unfortunately, this method merges two effects that obey different laws, mass-dependent fractionation on the one hand and mass-independent fractionation by variable cup efficiencies on the other hand. It therefore shifts in different directions and by different increments the measured values with respect to the true values in the space of isotopic ratios. These independent effects cannot be described by a single measurement. Therefore, we here develop new systems of equations that are versatile, relax the restrictions on the mass fractionation law, and lend themselves to easy error assessment through matrix analysis. Let us start by rewriting Eqn. 47 in a log form:

$$\ln r_i = \ln \mathcal{A}_{\alpha} - \ln \mathcal{A}_{\gamma} + (M_i^q - M_k^q) \ln h + \ln R_i \quad (49)$$

with the usual exponential-form limit when $q \to 0$:

$$\ln r_i = \ln \mathcal{A}_{\alpha} - \ln \mathcal{A}_{\gamma} + \beta \ln \frac{M_i}{M_k} + \ln R_i \quad (50)$$

When written in full, the number of unknowns is the sum $c + e + r$, where c is the number of active cups, e the number of elements for which the value h is needed, and r the number of ratios to measure. We further assume that q is known, but this condition can be relaxed at the price of increasing the number of unknowns by one.

We first show how to use a standard solution (or a mixture of

standards of different elements) of known isotopic compositions N_i/N_k to determine the cup efficiencies. The unknowns are the efficiencies $\mathcal{A}$ for each cup and the mass fractionation factors β (or h for other laws). The system of equations is particularly compact since Eqn. 50 now reduces to:

$$\ln \frac{r_i}{R_i} = \ln \mathcal{A}_\alpha - \ln \mathcal{A}_\gamma + \beta \ln \frac{M_i}{M_k} \tag{51}$$

This system can be conveniently written in a matrix form:

$$\mathbf{y} = \mathbf{A}\mathbf{x} \tag{52}$$

where the lower-case symbols stand for vectors ($\mathbf{x}$ for the unknowns $\mathbf{x} = \ln \mathcal{A}_\alpha \ldots \ln \mathcal{A}_\gamma$, β, and $\mathbf{y}$ for the data) and the upper-case symbol $\mathbf{A}$ for a rectangular matrix. In most cases, the number of measurements (dimension of $\mathbf{y}$) is larger than the number of unknowns (dimension of $\mathbf{x}$) and Eqn. 52 can be solved by standard least-square methods giving $\mathbf{x} = (\mathbf{A}^T \mathbf{A})^{-1} \mathbf{A}^T \mathbf{y}$. The errors on the unknown values x can simply be computed from the diagonal entry of $\mathbf{W_x} = (\mathbf{A}^T \mathbf{W_y}^{-1} \mathbf{A})^{-1}$, where $\mathbf{W_y}$ is the covariance matrix of the measurements $\mathbf{y}$. In most cases, an approximation of $\mathbf{W_y}$ by a diagonal matrix, in which the entries are the squared "errors", is sufficient.

Let us illustrate this method with the three-sequence dynamic run of a Pb-Tl mixture as described in Table 1 and assume for brevity that the exponential law holds. Efficiencies are known only as relative values and, for simplicity, we will assume that the efficiency factor of the axial cup is unity. For the best possible precision, the ratios to be measured are $^{205}Tl/^{203}Tl$, $^{206}Pb/^{204}Pb$, $^{207}Pb/^{206}Pb$, and $^{208}Pb/^{206}Pb$. The efficiencies will be evaluated for the cups L2, L1, H1, and H2. The mass fractionation coefficients β^{Pb} and β^{Tl} are assumed to be different.

Table 1. Sample configuration of dynamic Pb isotope analysis in three sequences. Faraday cups are labeled L for low masses, H for high masses, and Ax for the axial collector. The axial cup is the reference so its efficiency is assumed to be unity.

Sequence	L2	L1	(Ax)	H1	H2	H3
1	202	203	(204)	205	206	207
2	203	204	(205)	206	207	208
3	204	205	(206)	207	208	

$$\begin{vmatrix} \ln \frac{(^{205}Tl/^{203}Tl)_1^{meas}}{(^{205}Tl/^{203}Tl)_1^{ref}} \\ \ln \frac{(^{206}Pb/^{204}Pb)_1^{meas}}{(^{206}Pb/^{204}Pb)_1^{ref}} \\ \ln \frac{(^{207}Pb/^{206}Pb)_1^{meas}}{(^{207}Pb/^{206}Pb)_1^{ref}} \\ \ln \frac{(^{205}Tl/^{203}Tl)_2^{meas}}{(^{205}Tl/^{203}Tl)_2^{ref}} \\ \ln \frac{(^{206}Pb/^{204}Pb)_2^{meas}}{(^{206}Pb/^{204}Pb)_2^{ref}} \\ \ln \frac{(^{207}Pb/^{206}Pb)_2^{meas}}{(^{207}Pb/^{206}Pb)_2^{ref}} \\ \ln \frac{(^{206}Pb/^{204}Pb)_3^{meas}}{(^{206}Pb/^{204}Pb)_3^{ref}} \\ \ln \frac{(^{207}Pb/^{206}Pb)_3^{meas}}{(^{207}Pb/^{206}Pb)_3^{ref}} \\ \ln \frac{(^{208}Pb/^{206}Pb)_3^{meas}}{(^{208}Pb/^{206}Pb)_3^{ref}} \end{vmatrix} = \begin{vmatrix} 0 & -1 & 1 & 0 & 0 & \ln \frac{M_{205Tl}}{M_{203Tl}} & 0 \\ 0 & 0 & 0 & 1 & 0 & 0 & \ln \frac{M_{206Pb}}{M_{204Pb}} \\ 0 & 0 & 0 & -1 & 1 & 0 & \ln \frac{M_{207Pb}}{M_{206Pb}} \\ -1 & 0 & 0 & 0 & 0 & \ln \frac{M_{205Tl}}{M_{203Tl}} & 0 \\ 0 & -1 & 1 & 0 & 0 & 0 & \ln \frac{M_{206Pb}}{M_{204Pb}} \\ 0 & 0 & -1 & 1 & 0 & 0 & \ln \frac{M_{207Pb}}{M_{206Pb}} \\ -1 & 0 & 0 & 0 & 0 & 0 & \ln \frac{M_{206Pb}}{M_{204Pb}} \\ 0 & 0 & 1 & 0 & 0 & 0 & \ln \frac{M_{207Pb}}{M_{206Pb}} \\ 0 & 0 & 0 & 1 & 0 & 0 & \ln \frac{M_{208Pb}}{M_{206Pb}} \end{vmatrix} \begin{vmatrix} \ln \mathcal{A}_{L2} \\ \ln \mathcal{A}_{L1} \\ \ln \mathcal{A}_{H1} \\ \ln \mathcal{A}_{H2} \\ \ln \mathcal{A}_{H3} \\ \beta_{Tl} \\ \beta_{Pb} \end{vmatrix} \tag{53}$$

In the present case, the system has more equations (9) than unknowns (7) and may be conveniently solved for $\mathbf{x} = \mathcal{A}_{L2} \ldots \mathcal{A}_{H3}$, β_{T1}, and β_{Pb} by the least-square solution alluded to above.

The most useful extension of this method cuts down on the very cumbersome equations normally used for dynamic measurements of isotope compositions. The unknown isotopic ratios are added to the unknowns. For Nd isotope analysis, we may assume for example that $^{146}Nd/^{144}Nd$ is normalized to 0.7219 and use the cup configuration described in Table 2. We obtain the following system of linear equations in seven unknowns ($\mathcal{A}_{L2}$, $\mathcal{A}_{L1}$, $\mathcal{A}_{H1}$, β_{Nd}, and the corrected values of $^{142}Nd/^{144}Nd$, $^{143}Nd/^{144}Nd$, and $^{145}Nd/^{144}Nd$) to be solved by least-squares:

Table 2. A sample configuration for dynamic Nd isotope analysis in three sequences. Focusing and peak centering are carried out on the second sequence configuration.

Sequence	L2	L1	(Ax)	H1
1	142	143	(144)	145
2	143	144	(145)	146
3	144	145	(146)	

$$\begin{vmatrix} \ln\left(\frac{^{142}Nd}{^{144}Nd}\right)_1^{meas} \\ \ln\left(\frac{^{143}Nd}{^{144}Nd}\right)_1^{meas} \\ \ln\left(\frac{^{145}Nd}{^{144}Nd}\right)_1^{meas} \\ \ln\left(\frac{^{143}Nd}{^{144}Nd}\right)_2^{meas} \\ \ln\left(\frac{^{145}Nd}{^{144}Nd}\right)_2^{meas} \\ \ln\frac{(^{146}Nd/^{144}Nd)_2^{meas}}{0.7219} \\ \ln\left(\frac{^{145}Nd}{^{144}Nd}\right)_3^{meas} \\ \ln\frac{(^{146}Nd/^{144}Nd)_3^{meas}}{0.7219} \end{vmatrix} = \begin{vmatrix} 1 & 0 & 0 & \ln\left(\frac{M_{142Nd}}{M_{144Nd}}\right) & 1 & 0 & 0 \\ 0 & 1 & 0 & \ln\left(\frac{M_{143Nd}}{M_{144Nd}}\right) & 0 & 1 & 0 \\ 0 & 0 & 1 & \ln\left(\frac{M_{145Nd}}{M_{144Nd}}\right) & 0 & 0 & 1 \\ 1 & -1 & 0 & \ln\left(\frac{M_{143Nd}}{M_{144Nd}}\right) & 0 & 1 & 0 \\ 0 & -1 & 0 & \ln\left(\frac{M_{145Nd}}{M_{144Nd}}\right) & 0 & 0 & 1 \\ 0 & -1 & 1 & \ln\left(\frac{M_{146Nd}}{M_{144Nd}}\right) & 0 & 0 & 0 \\ -1 & 1 & 0 & \ln\left(\frac{M_{145Nd}}{M_{144Nd}}\right) & 0 & 0 & 1 \\ -1 & 0 & 0 & \ln\left(\frac{M_{146Nd}}{M_{144Nd}}\right) & 0 & 0 & 0 \end{vmatrix} \begin{vmatrix} \ln \mathcal{A}_{L2} \\ \ln \mathcal{A}_{L1} \\ \ln \mathcal{A}_{H1} \\ \beta_{Nd} \\ \ln\left(\frac{^{142}Nd}{^{144}Nd}\right)^{corr} \\ \ln\left(\frac{^{143}Nd}{^{144}Nd}\right)^{corr} \\ \ln\left(\frac{^{145}Nd}{^{144}Nd}\right)^{corr} \end{vmatrix} \quad (54)$$

On 10 measurements of the La Jolla Nd standard, we obtained the results listed in Table 3. The $^{142}Nd/^{144}Nd$, $^{143}Nd/^{144}Nd$, and $^{145}Nd/^{144}Nd$ ratios agree within error bars with literature values (Wasserburg et al., 1981). The larger errors obtained on the $^{142}Nd/^{144}Nd$ ratio result from (1) the much smaller amount of data collected for this ratio, which appears only in the first sequence, (2) the measurement of mass 142 on this shifted sequence while the peaks are focused and centered in the configuration of the second sequence, and (3) the unfavorable propagation of errors on this ratio. The exponentially corrected $^{142}Nd/^{144}Nd$ and $^{143}Nd/^{144}Nd$ ratios are strongly correlated with a correlation coefficient of 0.95, and the slope of the correlation (≈0.2) suggests that the second-order correction described by Eqn. 43 is applicable. Such a second step leaves the mean values essentially unchanged, but improves the precision by a factor of three on $^{143}Nd/^{144}Nd$ and a factor of two on $^{145}Nd/^{144}Nd$. If the slope of the correlation between standard values is used, as in Thirlwall (1991) and Vance and Thirlwall (2002), the gain in precision is comparable.

The system described above for Pb isotope measurements can be expanded by treating the $^{206}Pb/^{204}Pb$ and $^{207}Pb/^{206}Pb$ of the standard as unknown variables. As Doucelance and Manhès (2001), we assume that the less variable $^{208}Pb/^{206}Pb$ ratio is constant, but, contrary to these authors, we adopt the value of 2.1677, which is more consistent with double- and triple-spike results. The system of linear equations becomes:

$$\begin{vmatrix} \ln\frac{(^{205}Tl/^{203}Tl)_1^{meas}}{(^{206}Tl/^{203}Tl)_1^{ref}} \\ \ln\left(\frac{^{206}Pb}{^{204}Pb}\right)_1^{meas} \\ \ln\left(\frac{^{207}Pb}{^{206}Pb}\right)_1^{meas} \\ \ln\frac{(^{205}Tl/^{203}Tl)_2^{meas}}{(^{205}Tl/^{203}Tl)_2^{ref}} \\ \ln\left(\frac{^{206}Pb}{^{204}Pb}\right)_2^{meas} \\ \ln\left(\frac{^{207}Pb}{^{206}Pb}\right)_2^{meas} \\ \ln\left(\frac{^{206}Pb}{^{204}Pb}\right)_3^{meas} \\ \ln\left(\frac{^{207}Pb}{^{206}Pb}\right)_3^{meas} \\ \ln\frac{(^{208}Pb/^{206}Pb)_3^{meas}}{(^{208}Pb/^{206}Pb)_3^{ref}} \end{vmatrix} = \begin{vmatrix} 0 & -1 & 1 & 0 & 0 & \ln\frac{M_{205Tl}}{M_{203Tl}} & 0 & 0 & 0 \\ 0 & 0 & 0 & 1 & 0 & 0 & \ln\frac{M_{206Pb}}{M_{204Pb}} & 1 & 0 \\ 0 & 0 & 0 & -1 & 1 & 0 & \ln\frac{M_{207Pb}}{M_{206Pb}} & 0 & 1 \\ -1 & 0 & 0 & 0 & 0 & \ln\frac{M_{205Tl}}{M_{203Tl}} & 0 & 0 & 0 \\ 0 & -1 & 1 & 0 & 0 & 0 & \ln\frac{M_{206Pb}}{M_{204Pb}} & 1 & 0 \\ 0 & 0 & -1 & 1 & 0 & 0 & \ln\frac{M_{207Pb}}{M_{206Pb}} & 0 & 1 \\ -1 & 0 & 0 & 0 & 0 & 0 & \ln\frac{M_{206Pb}}{M_{204Pb}} & 1 & 0 \\ 0 & 0 & 1 & 0 & 0 & 0 & \ln\frac{M_{207Pb}}{M_{206Pb}} & 0 & 1 \\ 0 & 0 & 0 & 1 & 0 & 0 & \ln\frac{M_{208Pb}}{M_{206Pb}} & 0 & 0 \end{vmatrix} \begin{vmatrix} \ln \mathcal{A}_{L2} \\ \ln \mathcal{A}_{L1} \\ \ln \mathcal{A}_{H1} \\ \ln \mathcal{A}_{H2} \\ \ln \mathcal{A}_{H3} \\ \beta_{Tl} \\ \beta_{Pb} \\ \ln\left(\frac{^{206}Pb}{^{204}Pb}\right)^{corr} \\ \ln\left(\frac{^{207}Pb}{^{206}Pb}\right)^{corr} \end{vmatrix} \quad (55)$$

Table 3. Comparison with literature data of 10 dynamic runs of the La Jolla Nd standard on the MC-ICPMS (Plasma 54) of Lyon after normalization to $^{146}Nd/^{144}Nd = 0.7219$. Each run represents about 45 min of acquisition with the three sequences measured 60 times each with a settling time of 10 s.

	Lyon	Caltech	RHBC
Method	ICPMS	TIMS	ICPMS
A_{L2}	0.998314 (226)		
A_{L1}	0.999950 (69)		
A_{H1}	1.000317 (47)		
β_{Nd}	2.38 (0.03)		
$^{142}Nd/^{144}Nd^a$	1.141834 (321)	1.141827	1.141509 (63)
$^{143}Nd/^{144}Nd^a$	0.511853 (54)	0.511861	
$^{143}Nd/^{144}Nd^b$	0.511859 (17)		
$^{143}Nd/^{144}Nd^c$	0.511852 (17)		0.511856 (13)
$^{145}Nd/^{144}Nd^a$	0.348414 (17)	0.348415	
$^{145}Nd/^{144}Nd^b$	0.348413 (9)		
$^{145}Nd/^{144}Nd^c$			0.348421 (9)

ICPMS = inductively coupled plasma mass spectrometry; RHBC = Royal Holloway Bedford College; TIMS = thermal ionization mass spectrometry.

[a] One-stage mass fractionation correction using an exponential lau

[b] Second-order mass fractionation correction using the second-order correction of Eqn. 43.

[c] Two-stage mass fractionation correction based on the correlation between the first-stage values of $^{142}Nd/^{144}Nd^a$ and $^{143}Nd/^{144}Nd^a$ and a normalization to $^{142}Nd/^{144}Nd^a = 1.14187$ (Thirlwall, 1991; Vance and Thirlwall, 2002) The first-stage precision on the $^{142}Nd/^{144}Nd$ ratio is inferior to that on the other ratios because mass 142 is measured only once every third sequence and only in a shifted sequence (Table 2). For the Lyon column, errors in parentheses represent twice the unweighted standard deviation of the 10 individual run values. TIMS data from Wasserburg et al. (1981). RHBC data are from Vance and Thirlwall (2002).

On 10 measurements of the NIST 981 Pb standard solution taken in the present study as an example, we obtain $^{206}Pb/^{204}Pb$, $^{207}Pb/^{204}Pb$, and $^{207}Pb/^{206}Pb$ values consistent with the triple-spike TIMS values of Mainz (Eisele et al., 2002), the double-spike MC-ICPMS and TIMS values of Egham (Thirlwall, 2002), and the high-precision TIMS data of Paris (Doucelance and Manhès, 2001) (Table 4). In addition, we confirm through this calculation that the mass fractionation factors of Pb and Tl are indeed different. This difference, which is commonly on the order of 5% to 10%, varies from day to day and is large enough to account for the poor reproducibility of Pb isotope measurements obtained with the assumption that Pb and Tl have identical fractionation factors (Belshaw et al., 1998; Rehkämper and Mezger, 2000; Thirlwall, 2002). The difference between β_{Pb} and β_{Tl} (0.033 ± 21) produces a bias of ca. 160 ppm per unit of mass difference, which is comparable to the bias reported by the aforementioned authors between straightforward "Tl spiking" and other methods, including the use of a double-spike. The bias recorded with Tl spiking is therefore not the result of a deficiency of the MC-ICPMS instrument itself, but is rather due to the inadequacy of the assumption of a common extent of fractionation for Pb and Tl (Maréchal et al., 1999; White et al., 2000). It is quite satisfactory that once the ratios have been corrected for mass fractionation and cup efficiencies, a plot of $^{207}Pb/^{204}Pb$ vs. $^{206}Pb/^{204}Pb$ shows correlated ratios with a slope of ≈ 1, whereas a plot of $^{207}Pb/^{206}Pb$ vs. $^{204}Pb/^{206}Pb$ shows no correlation at all (Fig. 7). We will see below that this is a strong indication that variation is dominated by counting statistics and not by residual mass fractionation. Assuming that the Lu and Yb isotope compositions obtained by TIMS are not fractionated by more than a few per mil, the difference in β between the two neighboring elements is in excess of 50%, which we ascribe primarily to the greatly different ionization energies. The fluctuation of this difference, if not properly dealt with, is a source of uncertainty on the values of Lu concentrations obtained by isotope dilution (Blichert-Toft et al., 2002).

8. MEMORY EFFECTS

Background from previous runs varies from instrument to instrument, from laboratory to laboratory, and from day to day. For example, on the Plasma 54 in Lyon, we found that switching between the two Pb isotope standards NIST 981 and NIST 982 degrades the precision, which simply reflects that their

Table 4. Comparison of dynamic runs (February–July 2003) of the Pb NIST 981 standard on the MC-ICPMS (Plasma 54) of Lyon after normalization to $^{208}Pb/^{206}Pb = 2.1677$ with triple-spike results from Mainz (Eisele et al., 2002), Egham (Thirlwall, 2002), IPG Paris (Doucelance et al., 2001), and Brisbane (Collerson et al., 2002). Errors in parentheses represent twice the unweighted standard deviation of the individual run values.

Laboratory	Lyon			Mainz	RHBC	Paris	Brisbane
Instrument	ICP-MS			DS TIMS	DS ICP-MS	TIMS	ICP-MS Tl doping
run #	10	20	20				
A_{L2}	0.99982 (6)	1.00031 (15)	1.00017 (17)				
A_{L1}	1.00041 (13)	1.00051 (11)	1.00061 (9)				
A_{H1}	0.99912 (17)	1.00064 (34)	1.00106 (18)				
A_{H2}	0.99803 (29)	1.00056 (38)	1.00086 (26)				
A_{H3}	0.99667 (28)	0.99953 (36)	0.99972 (31)				
β_{T1}	1.928 (49)	2.005 (26)	1.877 (35)				
β_{Pb}	1.896 (47)	1.897 (30)	1.775 (37)				
$^{206}Pb/^{204}Pb$	16.9435 (30)	16.9434 (27)	16.9418 (27)	16.9425 (19)	16.9417 (29)	16.9406 (15)	16.941 (6)
$^{207}Pb/^{204}Pb$	15.5007 (27)	15.5003 (25)	15.4994 (25)	15.4998 (24)	15.4996 (31)	15.4988 (?)	
$^{207}Pb/^{206}Pb$	0.914845 (23)	0.914832 (16)	0.914865 (14)	0.914846	0.91488 (8)	0.91489 (2)	0.91466 (12)

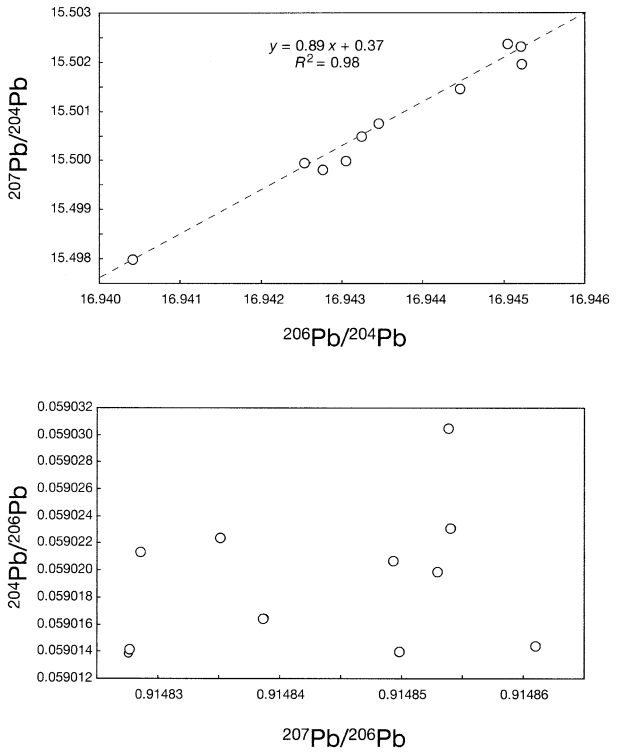

Fig. 7. A plot of $^{207}Pb/^{206}Pb$ vs. $^{204}Pb/^{206}Pb$ (bottom) corrected for mass fractionation for the 10 dynamic runs of Table 4 shows no residual correlation, which would reveal that the mass bias has not been adequately accounted for. In contrast, the plot of $^{207}Pb/^{204}Pb$ vs. $^{206}Pb/^{204}Pb$ (top) corrected for mass fractionation shows a strong correlation, which is due to the poor counting statistics on the smaller isotope 204.

isotopic compositions are very different. We found similar effects for Tl, when we tried to alternate a standard with natural isotopic proportions (i.e., rich in ^{205}Tl) and samples spiked with ^{203}Tl. At least for these two "sticky" elements, the instrument can never be completely cleaned over the time allocated to cleaning, which is typically 10–15 mn maximum.

It has been suggested that the On-Peak Zero (OPZ) procedure, which is the measurement of a blank solution before sample or standard analysis, can be used as a reference to correct for memory (e.g., Collerson et al., 2002; Thirlwall, 2002). We contend that memory is highly unstable and even OPZ does not account well enough for its isotopic composition to warrant high-precision measurements. The following example is taken from a recent attempt made in Lyon to compare the ^{204}Pb-^{207}Pb double-spike and the Tl doping methods. The washout solution of a heavily spiked sample was analyzed for 25 min through different rinse solutions, first concentrated (0.65 N) nitric acid, then dilute hydrofluoric acid, and then again concentrated nitric acid (Fig. 8). Hydrofluoric acid is helpful in removing a thin layer from the contaminated glassware. Returning next to the dilute nitric acid (0.05 N, not shown) used for sample and standard analysis, the blank at each mass was brought into the 10^{-16} A range, indistinguishable from the blank in dilute HF. At first sight, this result seems excellent, since the original sample signal is reduced by 5–6 orders of magnitude. The instrument blank should therefore be negligible with respect to any sample run right after such a cleaning procedure. The memory level of the Plasma 54 is at least an order of magnitude lower than the level quoted for some Isoprobe instruments (Thirlwall, 2002; Collerson et al., 2002). The situation seems less favorable for the 204 signal: this, however, cannot be attributed to residual mercury as the 202 signal is observed to decrease together with the heavier Pb isotopes. Rather, various "species" in the memory with different isotope compositions appear to be present and reacting differently to different cleaning media. The assumption that the level of signal at which these isotopic variations exist is too low to affect sample runs is incorrect: alternating spiked and unspiked standard solutions demonstrates that the presence of Pb in the solution enhances the leaching of a component that was not visible in the post-wash blank (Fig. 9). The result is a significant isotopic drift, both from spiked to unspiked and from unspiked to spiked runs. The seriousness of this memory problem is exacerbated by the fact that it is the rare isotope ^{204}Pb which is used as a spike. As shown in the bottom panel of Fig. 9, this problem does not exist for unspiked rock samples, namely when using the Tl doping technique.

Although such memory effects are not critical for isotope dilution measurements aiming at 2–5 per mil precision, they may have an adverse effect on the accuracy and precision of isotopic compositions in the 100 ppm range. The intensities of the background peaks are not reproducible since they depend on the recent history of a particular mass spectrometer. Let us consider the case of Pb isotope measurements when samples doped with Pb double spike with a high ^{204}Pb abundance are routinely run on the same instrument. A 2 10^{-16} A beam equivalent to a 20-μV signal on a standard 10^{11} Ω resistor would still be within the thermal (Johnson) noise of the resistor and therefore escape detection on a Faraday cup. In comparison, a 7-V total signal of normal lead would come with about 100 mV at mass 204 and memory would contribute with a bias of about 200 ppm to ^{204}Pb. Because the 204 isotope in Pb double spike is fairly abundant, the bias rapidly becomes significant. For example, expressing that the raw (total) ^{206}Pb and ^{204}Pb signals are the sum of a sample and a background signal, we get

$$\left(\frac{^{206}Pb}{^{204}Pb}\right)^{total} = \left(\frac{^{206}Pb}{^{204}Pb}\right)^{sple} + \left[\left(\frac{^{206}Pb}{^{204}Pb}\right)^{bkgd} - \left(\frac{^{206}Pb}{^{204}Pb}\right)^{sple}\right]\frac{^{204}Pb^{bkgd}}{^{204}Pb^{total}} \quad (56)$$

Not correcting the apparently negligible contribution of the background would create a bias of

$$\frac{\Delta^{206}Pb/^{204}Pb}{(^{206}Pb/^{204}Pb)^{sple}} = \left[\frac{(^{206}Pb/^{204}Pb)^{bkgd}}{(^{206}Pb/^{204}Pb)^{sple}} - 1\right]\frac{^{204}Pb^{bkgd}}{^{204}Pb^{total}} \quad (57)$$

In the particular case just discussed, the requirement of <50 ppm bias necessitates that both the $^{206}Pb/^{204}Pb$ ratio of the background and the $^{204}Pb^{bkgd}/\,^{204}Pb^{total}$ ratio be known *for this particular run* with a precision of 25%, which is a difficult goal to achieve on such a small signal. Isobaric interferences, such as ^{204}Hg on ^{204}Pb, and the coexistence of several memory "species" with different isotope compositions complicate matters even further, in particular when complex desolvating sys-

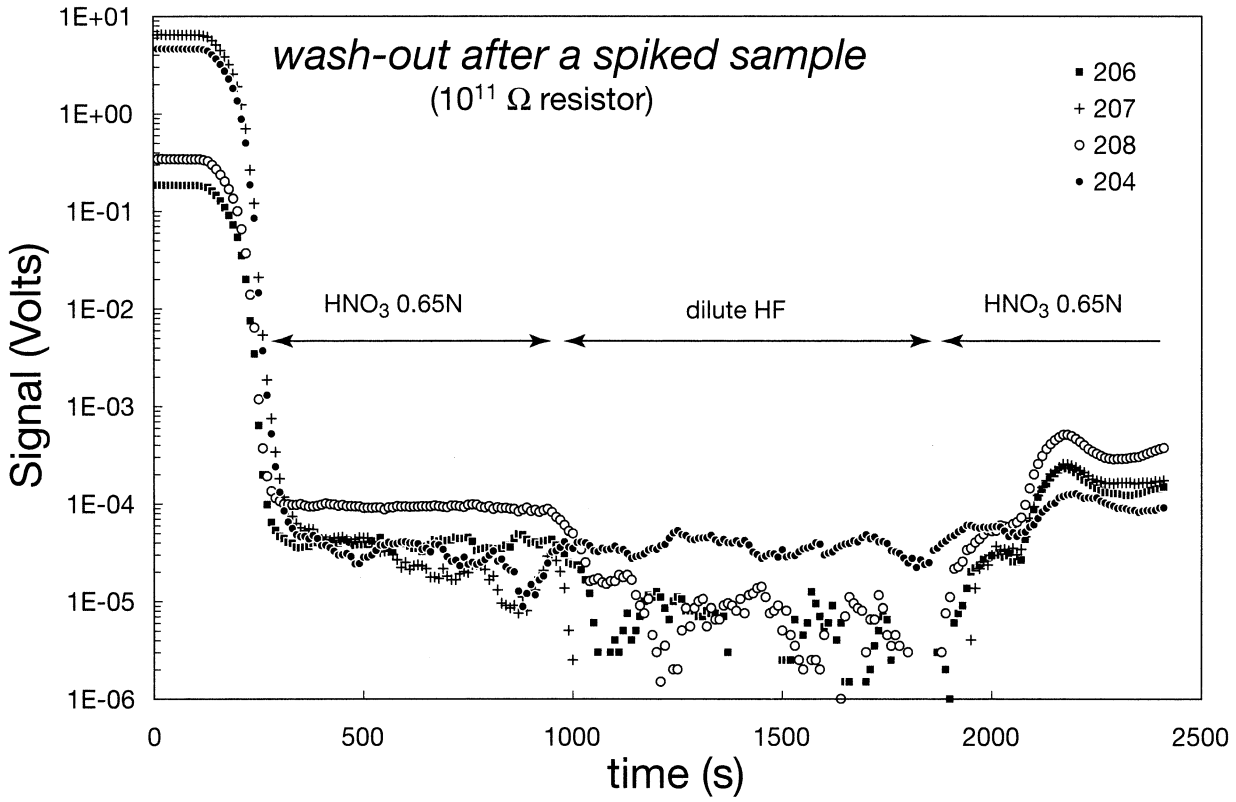

Fig. 8. Wash-out of a Pb NIST 981 standard sample spiked with ^{204}Pb and ^{207}Pb. Open symbols: outliers at the 95% confidence level. Concentrated nitric acid removes most of the signal within a few minutes. Dilute hydrofluoric acid intended to strip off the contaminated surface of the glassware lowers the residual signal further down to a level similar to that found in the dilute nitric acid (0.05 N) used for sample analysis. With concentrated nitric acid (0.65 N), the blank level bounces back. The signal of the wash-out solution therefore seems negligible with respect to the usual signal routinely obtained on rock samples. Note the large changes in apparent ^{204}Pb/^{208}Pb ratios for different acids. The small residual signal at mass 204 is not due to mercury, since the 202 signal is essentially suppressed, but shows that memory contains several "species" with different isotope compositions. This problem is only present for samples spiked with ^{204}Pb.

tems are used, which offer many potential sites and mechanisms of contamination. The amount of mercury present in argon may vary from batch to batch. In the blank of the Plasma 54 of Lyon, Hg contributes to less than 10^{-4} of the residual 204 signal (e.g., White et al., 2000) which, as shown above, is very small, while this proportion can reach several percent on other instruments (Thirlwall, 2002; Collerson et al., 2002). Again, using the OPZ for correction will only help if the Hg/Pb ratio and the Pb isotope composition of the memory signal can be clearly demonstrated to remain constant upon sample introduction. Assessing the impact of an imperfect knowledge of the memory on double-spike and dynamic methods is a particularly daunting challenge.

9. COUNTING STATISTICS

The central assumption of ion counting is that ions arrive at the detector "at random", i.e., that the probability of arrival of an ion is the same for any time interval of a same length. The number n_i of ions i arriving at any collection device during the time interval δt is therefore subject to Poisson statistics: n_i is proportional to δt, the average count rate is $n_i/\delta t$, and its variance is also equal to $n_i/\delta t$. The standard deviation of an ion beam I_i measured in ions per second is proportional to the square-root of the beam intensity and the relative error is $\sqrt{I_i}/I_i = 1/\sqrt{I_i}$. Smaller beams therefore fluctuate more than larger beams. The noise due to counting statistics, known as shot noise, accounts for a 250 ppm (2σ level) error on a typical 1-V signal collected in 1 s through a 1 Ω resistor or in 10 s on a 100-mV signal. This noise is not to be confused with the thermal (Johnson) noise of the resistor $\sigma_A^2 \approx 4kT/R\Delta t$ where k is the Boltzmann constant, T the temperature, R the resistance, and Δt the integration interval (Nyquist, 1928). Shot noise imposes strong correlations on some isotopic plots that may easily be mistaken for mass-dependent fractionation effects. This is a familiar problem for Pb in particular (e.g., Hamelin et al., 1985; Powell et al., 1998) because of the common usage of the minor ^{204}Pb isotope as the reference isotope, but it exists to a variable extent for all elements. Let us consider two measured isotopic ratios $r_i = n_i/n_k$ and $r_j = n_j/n_k$. Taking the first-order expansion of $\ln r_i$ around its mean value (noted by an overbar) gives:

$$\frac{n_i/n_k - \overline{n_i/n_k}}{n_i/n_k} \approx \frac{n_i - \bar{n}_i}{n_i} - \frac{n_k - \bar{n}_k}{n_k} \tag{58}$$

with a similar expression for r_j. By squaring these two expres-

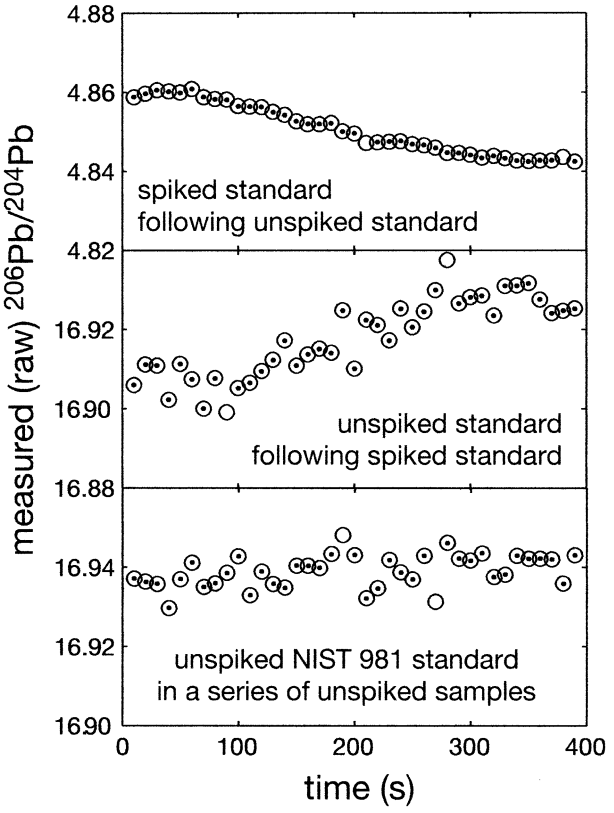

Fig. 9. Evidence that Pb memory is enhanced by introducing a Pb solution into the mass spectrometer. The instrument is thoroughly cleaned using the protocol illustrated in Fig. 8 until the total Pb signal is reduced to less than 10^{-15} A (0.1 mV). Standard solutions of NIST 981 Pb either unmodified or spiked with a ^{204}Pb-^{207}Pb tracer are then introduced into the mass spectrometer. The total Pb signal is typically in the range of 10^{-11} to 10^{-10} A (1–10 V). Despite thorough cleaning, enough memory is present to induce a significant drift in isotopic ratios. Bottom panel: switching between samples with similar isotopic ratios does not show this problem.

sions, taking their expectation, and noting that statistical noise on different peaks is independent, we obtain:

$$\frac{\mathrm{var}(r_i)}{(r_i)^2} \approx \frac{\mathrm{var}(n_i)}{n_i^2} + \frac{\mathrm{var}(n_k)}{n_k^2} = \frac{1}{n_i} + \frac{\sigma_A^2}{n_i^2} + \frac{1}{n_k} + \frac{\sigma_A^2}{n_i^2} \quad (59)$$

with a similar expression for n_j/n_k. The covariance between the ratios is similarly:

$$\frac{\mathrm{cov}\ (r_i,r_j)}{r_i r_j} \approx \frac{\mathrm{var}\ (n_k)}{n_k^2} = \frac{1}{n_k} \quad (60)$$

Because the emphasis of this section is on counting statistics, we will at this point consider that the thermal noise of the resistor can be neglected, which is an acceptable assumption for signals higher than about 10^{-12} A. For ratios with the same denominator, e.g., ^{204}Pb for ^{205}Pb/^{204}Pb and ^{207}Pb/^{204}Pb, the slope of the noise correlation line in a ratio-ratio

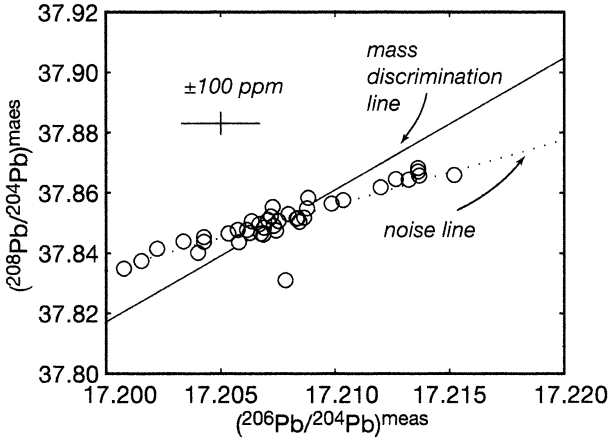

Fig. 10. Example of a strong noise-induced correlation observed on Pb isotopes within a block of 40 cycles. The solid line corresponds to mass-dependent fractionation, while the dotted line is defined by counting statistics and is essentially controlled by the small ^{204}Pb beam.

plot is the ratio of the standard deviations $\sigma_{j/k}$ and $\sigma_{i/k}$ along each axis (e.g., Albarède, 1995, p. 202):

$$\frac{\sigma_{j/k}}{\sigma_{i/k}} = \sqrt{\frac{r_j}{r_i}\frac{1+r_j}{1+r_i}} \quad (61)$$

while the correlation coefficient between the errors on the two ratios is:

$$\rho_{i/k}^{j/k} = \sqrt{\frac{r_i}{1+r_i} \times \frac{r_j}{1+r_j}} \quad (62)$$

Typical values of the correlation coefficients are 0.5 for two isotopic ratios equal to unity and quickly tend to unity for large ratios, such as ^{206}Pb/^{204}Pb, ^{207}Pb/^{204}Pb, and ^{208}Pb/^{204}Pb (Fig. 10). Correlations between errors due to counting statistics are clearly minimized by using ratios with values <1.

The slope $s_{i/k}^{j/k}$ of the noise correlation line in a log-log plot (or in an $\varepsilon - \varepsilon$ plot) is approximated by:

$$s_{i/k}^{j/k} = \sqrt{\frac{1+s_j}{s_j} \Big/ \frac{1+s_i}{s_i}} \quad (63)$$

These expressions are important for separating immediately the correlations between isotopic ratios introduced by mass-dependent discrimination from those introduced by mass-independent counting fluctuations. Residual correlations between the mass-bias corrected isotopic ratios and the mass-bias index are expected. A correlation with a slope equal to the difference between the slope of the noise line and that of the fractionation line is expected between the ratios corrected for mass bias, which should not necessarily be taken as an indication that the instrumental mass-fractionation law should be amended. For a number of systems, Table 5 lists the slopes between some critical ratios and the particular ratio used to assess the mass bias. A test for unambiguously separating the effect of counting statistics from that of instrumental mass discrimination is to plot isotopic ratios with no common isotope, e.g., ^{146}Nd/^{144}Nd vs. ^{145}Nd/^{142}Nd, ^{207}Pb/^{206}Pb vs. ^{208}Pb/^{204}Pb, or ^{206}Pb/^{204}Pb vs. ^{205}Tl/^{203}Tl (Fig. 11): any correlation in these diagrams must

Table 5. Comparison of apparent fractionation induced by counting statistics and mass-dependent bias.

			log-log slope	
x	y	ρ	noise	mass bias
$^{56}Fe/^{54}Fe$	$^{57}Fe/^{54}Fe$	0.50	1.87	1.49
$^{66}Zn/^{64}Zn$	$^{68}Zn/^{64}Zn$	0.32	1.14	1.97
$^{66}Zn/^{64}Zn$	$^{67}Zn/^{64}Zn$	0.17	2.17	1.49
$^{142}Nd/^{144}Nd$	$^{143}Nd/^{144}Nd$	0.43	1.25	0.50
$^{146}Nd/^{144}Nd$	$^{143}Nd/^{144}Nd$	0.38	1.11	−0.51
$^{146}Nd/^{144}Nd$	$^{142}Nd/^{144}Nd$	0.47	0.89	−1.01
$^{150}Nd/^{144}Nd$	$^{148}Nd/^{144}Nd$	0.19	1.01	1.49
$^{148}Nd/^{142}Nd$	$^{143}Nd/^{142}Nd$	0.23	0.75	0.17
$^{179}Hf/^{177}Hf$	$^{176}Hf/^{177}Hf$	0.31	1.39	−0.50
$^{179}Hf/^{177}Hf$	$^{180}Hf/^{177}Hf$	0.53	0.80	1.50
$^{206}Pb/^{204}Pb$	$^{208}Pb/^{204}Pb$	0.94	1.00	1.50
$^{206}Pb/^{204}Pb$	$^{207}Pb/^{204}Pb$	0.96	0.98	1.99
$^{204}Pb/^{206}Pb$	$^{207}Pb/^{206}Pb$	0.16	0.34	−0.50
$^{207}Pb/^{206}Pb$	$^{208}Pb/^{206}Pb$	0.57	0.84	2.00

be due to instrumental mass fractionation. Thus, the absence of correlations in plots of mass-fractionation corrected ratios with no common isotope shows that mass fractionation was corrected efficiently.

10. IMPROVING PRECISION BY POOLING RUNS

Making the standard error of the mean more precise by pooling runs is common practice in TIMS (Harper and Jacobsen, 1992), but has nevertheless occasionally been criticized (Sharma et al., 1996). The arguments against pooling notably involve observations of matrix effects and machine drift. Matrix effects can be rigorously handled by checking that sample solutions contain no detectable matrix, e.g., by running test samples on a quadrupole ICPMS across the entire mass range.

Effects of machine drift can be tested by comparing successive runs of the same solution and testing whether the set of isotopic deviations from one run to the next belongs to a single population, which, for convenience, will be assumed to be normal. The most powerful of normality tests is the quantile-quantile (QQ) plot, which involves comparing the sorted reduced residuals, i.e., (value-average)/standard deviation, between the measured samples and an ideal sample from a normal population with the same average and standard deviation (Fig. 12). Such a standard method (e.g., Johnson and Winchern, 1992) tests the "spacing" (inverse frequency) between the ordered residuals with respect to a normal population. We plotted the data for a 16-h period of Nd standard runs, during which both the $^{142}Nd/^{144}Nd$ and $^{143}Nd/^{144}Nd$ ratios were measured, and tested the normality of the relative deviation between successive standards. Because the isotopic compositions of rock samples are referred to the standard solution run immediately before and after, this test is crucial to the true method precision and should allow the analyst to decide whether the sample-standard deviations can be pooled within a single population. Each run takes a set of 80 measurements of 15 s each. We found that, during the 16-h period, the mean value of these deviations was −0.1 ppm with a standard deviation of 18 ppm for $^{142}Nd/^{144}Nd$ and 24 ppm for $^{143}Nd/^{144}Nd$. More significant is that these deviations form a normal population with a misfit from normality of less than a few ppm (Fig. 12). This observation demonstrates that sample runs can be pooled for improved precision without infringing on the assumption of a common population. Pooling is one of the bases for the precision of 10–15 ppm obtained on $^{142}Nd/^{144}Nd$ for 3.8 Ga old rocks from Greenland, that show evidence of the existence of short-lived ^{146}Sm in the early Earth (Boyet et al., 2003).

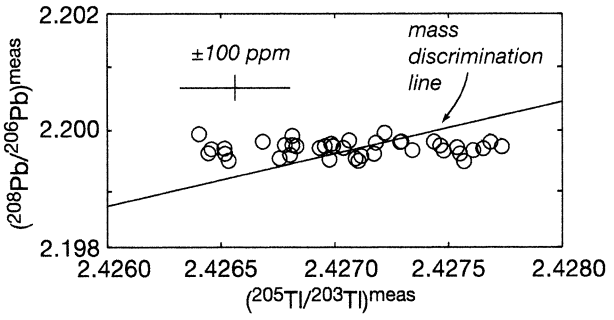

Fig. 11. When the ratios on each axis have no isotope in common and in the absence of mass-dependent fractionation, they are statistically independent. These data represent a run of 40 cycles, in which $^{206}Pb/^{204}Pb$ and $^{205}Tl/^{203}Tl$ were measured. The horizontal array (uncorrelated variables) indicates that, in the present case, the variability of the isotopic ratios can be ascribed to counting statistics and not to mass-dependent fractionation.

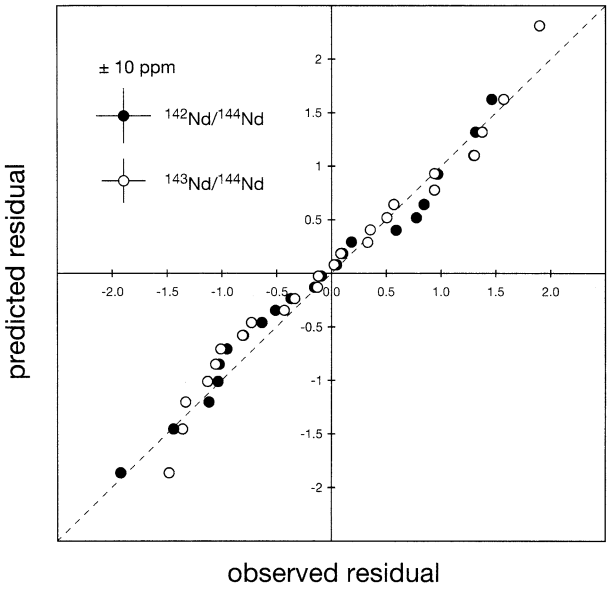

Fig. 12. Quantile-quantile (QQ) plot of isotope results on a Nd standard solution measured over a period of 16 hs. The variables to be tested are the deviations of the mean $^{142}Nd/^{144}Nd$ and $^{143}Nd/^{144}Nd$ of each run with respect to the mean of the preceding and following runs. The mean value of both variables is −0.1 ppm. The observed deviations are centered and reduced, then sorted in ascending order. The observed quantiles are compared with the theoretical quantiles predicted from a normal population with the same mean and variance. This plot demonstrates that the distribution of the sample-standard differences does not deviate from a normal population by more than a few ppm. This observation justifies the pooling of different runs for improved precision.

11. DISCUSSION

Vigorous discussion about the potential precision and accuracy of MC-ICPMS has been playing out in the literature over the last few years (e.g., Thirlwall, 2000, 2002). The advantage of TIMS instruments over MC-ICPMS remains the smaller mass fractionation of the former. Typical values of $\beta = 2$ are observed on some MC-ICPMS instruments, while others have a wider range. It is inevitable, however, that as improved transmission gets close to unity, mass fractionation diminishes (f and $\beta \rightarrow 0$). The bad news then become that mass fractionation will change with transmission, even with the same instrument configuration.

We consider, however, that if signal intensity is kept within a narrow range, MC-ICPMS should become the instrument of choice. Here we assert that in order to achieve high precision and accuracy, utmost care must be exercised to comply with a set of relatively simple rules:

(1) The matrix of samples must be reduced to trace amounts, typically of a far smaller total concentration than the element to be analyzed. This requirement is most critical when the mass bias is inferred, not internally from the sample itself, but externally from bracketing standards. Even the most dilute heavy species may drastically affect mass discrimination (Niu and Houk, 1996) and create interfering double-charged species (such as $^{48}Ca^{2+}$ on ^{24}Mg). Species lighter than the element may create molecular isobaric interferences with Ar, O, N, and C, such as $^{12}C_2$ on ^{24}Mg or $^{155}Gd^{16}O$ on ^{171}Yb. Evidence that a cold trap placed on the sample pathway efficiently removes species interfering with the Nd spectrum at the 10–100 ppm level has been presented elsewhere (Boyet et al., 2003).

(2) Cup efficiencies must be evaluated regardless of the instrument. In static mode, an incorrect isotopic composition of the standard changes the value of the mass fractionation coefficient and will harm accuracy if there is no reference ratio of stable isotopes. If cup factors are properly calibrated, e.g., by running a standard in either static or dynamic mode, accurate ratios can be retrieved from even a significantly biased array of Faraday cups. The method described in Blichert-Toft et al. (1997) and Luais et al. (1997) and based on Eqn. 10 is illustrated in Fig. 13. As shown in the introductory sections on mass fractionation, ln r_i/R_i should form a linear alignment when plotted against $M_i^q - M_k^q$. This can be illustrated for the exponential law, for which the abscissa is ln (M_i/M_k). The slope, which is calculated by linear regression so as to minimize the deviation of all the ratios from their accepted value, determines a mean fractionation factor $\bar{\beta}$. The residual for each mass is then ascribed to cup efficiencies. For Nd, $\bar{\beta}$ is different from the β_{146} inferred from the $^{146}Nd/^{144}Nd$ ratios. This method is essentially equivalent to selecting the mean fractionation coefficient $\bar{\beta}$, which would minimize the sum of the squared $\delta\beta_i$ values of Eqn. 44 over all the plotted isotopic ratios instead of normalizing with respect to a unique reference ratio. When only the deviation of the sample isotopic ratios from their values in the standard is sought (which covers most geochemical needs), an excellent external precision (15 ppm or less) competing with the precision achieved on TIMS is obtainable in static mode (Vance and Thirlwall, 2002; Boyet et al., 2003). The dynamic mode is the method of choice for accuracy and control, especially for Pb, but, as visible from Table 3, precision is heavily taxed because of excessively slow data acquisition. For Pb, the isotopic compositions of unknown samples cannot be obtained in dynamic mode without assuming that at least one ratio is known. We therefore rather suggest the use of an indirect ("vicarious") dynamic method: the cup efficiencies and the difference $\beta_{Pb} - \beta_{Tl}$ are determined from the compositions of the bracketing Pb standards run in dynamic mode, and these values are then used to correct the bracketed samples run in static mode. Table 6 shows some results obtained in vicarious mode on the NIST 981 Pb standard and on the CRPG basaltic rock standard BEN. Since the conditions of TIMS runs are variable from one sample to the next, essentially as a result of variable positions and temperatures of the hot spot on each filament, this method is restricted to MC-ICPMS measurements only.

(3) Memory must be assessed by running not only wash solutions but also a variety of elements, starting with the

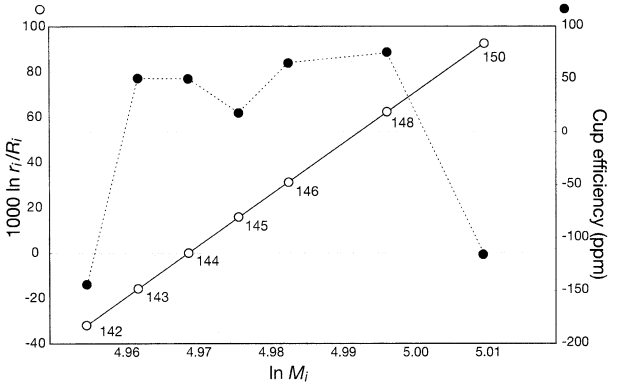

Fig. 13. The open circles represent the ratio between measured and "true" ratios. Isotope 144 is used as the reference, although this is not critical. A second-order correction of the mass bias is only requested at masses 142 and 150 because the cup efficiencies (solid symbols), which are essentially the residue after a least-square regression through the open symbols, do not vary smoothly with mass. The data shown are a block of 40 cycles measured on a standard solution. The cup efficiencies are only known relative to an arbitrary reference.

Table 6. Vicarious (indirect) dynamic measurements of NIST standard 981 and of the basalt rock standard BEN.[a]

n	NBS 981 8	BEN 6
$^{206}Pb/^{204}Pb$	16.9443 (47)	19.2363 (49)
$^{207}Pb/^{204}Pb$	15.5020 (50)	15.5994 (50)
$^{208}Pb/^{204}Pb$	36.734 (16)	39.038 (16)
$^{207}Pb/^{206}Pb$	0.91488 (11)	0.81094 (7)
$^{208}Pb/^{206}Pb$	2.16792 (53)	2.02939 (38)

[a] Every second measurement is a NIST 981 standard which is run in dynamic mode and used to determine cup efficiencies and a f_{Pb}/f_{Tl} ratio. These values are applied to the next sample (either another NIST 981 or Pb separated from the BEN rock standard) which is run in static mode. n-number of samples; the uncertainties in parentheses are two standard deviations.

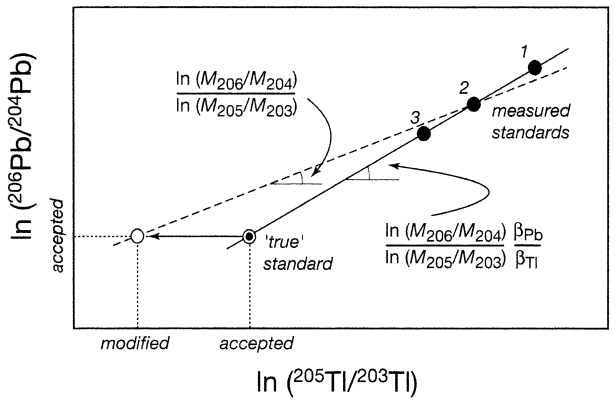

Fig. 14. Graphical description of the effect of changing the reference $^{205}Tl/^{203}Tl$ ratio of a standard solution used to normalize Pb isotope measurements (Rehkämper and Halliday, 1998) (sketchy and exaggerated). The measured $^{205}Tl/^{203}Tl$ and $^{206}Pb/^{204}Pb$ ratios of the standard solutions plot on the solid line for which $\beta_{Pb} \neq \beta_{Tl}$. In order to force $\beta_{Pb} = \beta_{Tl}$, the $^{205}Tl/^{203}Tl$ of the Tl spike solution is adjusted to plot on the dashed line for the "true" (accepted) value of the $^{206}Pb/^{204}Pb$ of the standard solution.

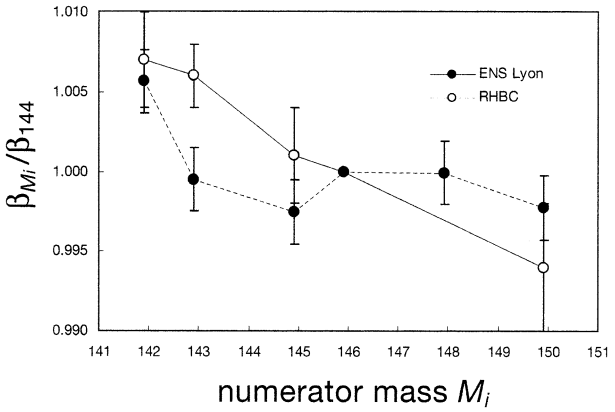

Fig. 15. Variation of $\beta = \ln (r_i/R_i)/ \ln (M_i/M_{144})$ as a function of M_i for two MC-ICPMS instruments, the Isoprobe of RHBC in Egham (Vance and Thirlwall, 2002) and the Plasma 54 in Lyon. T_i refers to raw measured ratios. The instrument in Lyon can be tuned to less distortion at mass 142, but this would be at the expense of performance at mass 150. The second-order correction term is proportional to the slope of the observed array (Eqn. 39). The quasi-linear array obtained in Egham is amenable to a smooth second-order correction of the mass bias. In contrast, such a correction is variable across the mass range on the Plasma 54 of Lyon.

element to be measured itself, that may enhance leaching in the entire instrumental setup (glassware, cones, plates). Double-spike techniques (Dodson, 1963; Hamelin et al., 1985; Galer, 1999) involve the addition of an isotope which is usually minor in natural samples, such as ^{204}Pb, implying that the risk introduced by memory effects on these spike isotopes must be carefully weighed against the added gain in precision from using the double spike (Woodhead, 2002). For Pb, memory is likely to jeopardize the quality of double- and triple-spike measurements because the abundances of the isotopes used for the spike are normally small in natural samples. Such a risk is clearly more present with MC-ICPMS than with TIMS, yet the dilemma familiar to many geochemistry groups applies to both techniques: is the analyst willing to commit routinely the *same* mass spectrometer to the isotopic analysis of Pb for zircon U-Pb dating *and* small amounts of unradiogenic Pb from meteorites? If the answer is negative, memory is certainly an issue. With respect to this problem, we contend that the T1 doping technique is viable with the caveat that alternating samples with similar isotope compositions will give more precise results than switching between samples with wildly variable isotope compositions.

(4) When mass discrimination is absolutely stable, standard bracketing is the method of choice. In other cases, however, mass discrimination can be evaluated using a second element (e.g., Tl on Pb, Cu on Zn, Yb on Lu), but the assumption that the two elements fractionate to the same extent is incorrect (Table 4) and results in systematic errors of a few hundred ppm or more (Rehkämper and Mezger, 1997; Thirlwall, 2002). Rehkämper and Halliday (1998) chose to alter the accepted value of the $^{205}Tl/^{203}Tl$ ratio, which amounts to forcing the accepted values onto a fractionation line with $\beta_{Pb} = \beta_{Tl}$ (Fig. 14). This practice does minimize short-term misfits on a particular instrument, but the modified $^{205}Tl/^{203}Tl$ ratio neither remains constant through time (Rehkämper and Mezger, 2000) nor agrees between different instruments (see an extensive discussion in Thirlwall, 2002), clearly reflecting that $\beta_{Pb} \neq \beta_{Tl}$. The above theory clearly indicates that such an artifice is not necessary. When mass fractionation varies too little for the slope of the mass fractionation line to be evaluated with precision, it still remains to be checked that stability is preserved upon introduction of rock samples: these are never totally matrix-free, even after a thorough purification chemistry. This can be conveniently tested by adding some of the elements present in the sample to a reference solution (Woodhead, 2002) or by running the same dissolution of a sample reasonably abundant in the element to be analyzed through distinct chemical extractions.

(5) The necessity of a second-order correction should be established by showing that the bias left after a first-order correction still depends smoothly on the mass or by testing the slope of the correlation between exponentially corrected ratios. A quasi-linear dependence of the exponential fractionation factor with mass indicative of second-order effects is clearly visible on some Isoprobe instruments (e.g., Fig. 3 in Vance and Thirlwall, 2002). On the Plasma 54 in Lyon (Fig. 15), a second-order correction using the $^{142}Nd/^{144}Nd$ ratio improves the precision of the $^{143}Nd/^{144}Nd$ data and, to a lesser extent, the $^{145}Nd/^{144}Nd$ and $^{148}Nd/^{144}Nd$ data as well. The second-order coefficient γ is, however, smaller at intermediate masses, thereby suggesting some degradation of transmission away from the optical axis of the instrument.

(6) A correlation between isotopic ratios corrected for mass fractionation may also reveal imperfectly-flat peak tops and effects of counting statistics, which are both mass-independent fractionation effects. The two-stage correction introduced by Thirlwall (1991) for Nd isotopic analysis, and applied by Vance and Thirlwall (2002) and Caro et al. (2003), handles both second-order effects and mass-inde-

pendent fractionation due to the peak shape surprisingly well (Fig. 6). A simple test, which still needs to be conducted on rock samples, would be to compare the results upon exchange of the order of normalization to the two reference isotope ratios. For the lack of more than two T1 isotopes, this method is unfortunately not applicable to lead.

(7) Abundance sensitivity (tailing) has been extensively discussed by Rehkämper and Mezger (2000), White et al. (2000), and Thirlwall (2002), among others, and seems to be an issue for Pb isotopes when Tl is used to correct mass fractionation on Pb. For Isoprobe instruments, Thirlwall (2002) quotes an abundance sensitivity of up to 25 ppm, while Rehkämper and Mezger (2000) show a change of Pb isotopic ratios with the Tl/Pb ratio. We found on the Plasma 54 of Lyon, for which the abundance sensitivity is about 2–5 ppm, that decreasing the Tl signal to the 10^{-12} A range and avoiding to measure zeroes on the tails of large peaks suffices to alleviate this problem.

12. CONCLUSIONS

Because of the complex trajectories of ion beams, obtaining precise and accurate isotopic data by MC-ICPMS still requires an adequate understanding of instrumental fractionation processes, both mass-dependent and mass-independent. In this paper, we have presented a unifying phenomenological theory for mass-dependent fractionation in mass spectrometers. Accuracy is related to what is known as cup efficiencies, but actually involves the complexity of ion paths. Although these can be calibrated by running known isotopic standards, we derive a straightforward, though very general method to calculate accurate ratios from dynamic measurements. Additional conclusions from this work are:

- The assumption of similar mass bias for neighboring elements (notably Pb and Tl, and Yb and Lu) is both unnecessary and incorrect.
- Straightforward standard-sample bracketing with no independent correction of the mass bias can only be applied when the sample and standard solutions are identical, which assumes near-perfect chemical separation procedures.
- Pooling runs to improve precision is an acceptable procedure provided the pooled measurements are shown to be part of a single population.
- Failure to produce flat-top peaks introduces a significant bias and spurious correlations between corrected ratios.
- Two-stage mass fractionation correction deals with both second-order effects and slightly imperfect peak tops and is capable of improving the ultimate precision of the measurements.
- Counting statistics introduce significant correlations, which should not be mistaken for residual mass fractionation effects.
- Because double-spike methods use minor isotopes, they are limited in precision by memory effects.

Repetitive calibration of cup efficiencies and rigorous assessment of mass bias combined with standard-sample bracketing are required for high-precision and accurate measurements by MC-ICPMS. We suggest that, once these simple guidelines are followed, MC-ICPMS is able to produce data precise and accurate to 15 ppm and possibly even better with the new generation of mass spectrometers.

Acknowledgments—This work represents the current know-how of ICPMS developed by many people over the past decade. We would like to thank those who contributed in our laboratory to some aspects of this development, notably Chantal Douchet for her constant help in the laboratory, students, former students, and coworkers Gry Hoffmann Barfod, Daniela Gasperini, Chloé Maréchal, Béatrice Luais, Frédéric Moynier, Sylvain Pichat, our countless visitors with a special mention of Dalila Ben Othman, Delphine Bosch, Barry Hanan, Jean-Marc Luck, Jeff Vervoort, Ivan Vlastelic, Dominique Weis, and Bill White. Reviews of the manuscript by Yuri Amelin, Clark Johnson, Felix Oberli, and Matthew Thirlwall helped identify inconsistencies, errors, and omissions and improved the manuscript substantially. The Institut des Sciences de l'Univers through Philippe Vidal and John Ludden and the Ministère de la Recherche provided stable funding of the Lyon MC-ICPMS operation and constant encouragements, both of which allowed us to embark on daunting projects with unpredictable outcomes. The manuscript was written during a leave of absence of F.A. and J.B.T. at Caltech. We thank the Moore Foundation (F.A.) and Caltech (J.B.T) for support.

Associate editor: Y. Amelin

REFERENCES

Albarède F. (1995) *Introduction to Geochemical Modeling*. Cambridge University Press.

Barfod G. H., Otero O., Albarède F. (2003) Phosphate Lu-Hf geochronology. *Chem. Geol.* **200,** 241–253.

Belshaw N. S., Freedman P. A., O'Nions R. K., Frank M., and Guoa Y. (1998) A new variable dispersion double-focusing plasma mass spectrometer with performance illustrated for Pb isotopes. *Int. J. Mass Spectrom.* **181,** 51–58.

Blichert-Toft J., Chauvel C., and Albarède F. (1997) Separation of Hf and Lu for high-precision isotope analysis of rock samples by magnetic sector-multiple collector ICP-MS. *Contrib. Mineral. Petrol.* **127,** 248–260.

Blichert-Toft J., Boyet M., Télouk P., and Albarède F. (2002) ^{147}Sm-^{143}Nd and ^{176}Lu-^{176}Hf in eucrites and the differentiation of the HED parent body. *Earth Planet. Sci. Lett.* **204,** 167–181.

Boyet M., Rosing M., Blichert-Toft J., Storey M., Télouk, P., and Albarède F. (2003) ^{142}Nd evidence for early Earth differentiation. *Earth Planet. Sci. Lett.* **214,** 427–442.

Caro C., Bourdon B., Birck J. L., and Moorbath S. (2003) ^{146}Sm ^{142}Nd evidence from Isua metamorphosed sediments for early differentiation of the Earth's mantle. *Nature* **423,** 428–432.

Collerson K. D., Kamber B. S., and Schoenberg R. (2002) Applications of accurate, high-precision Pb isotope ratio measurement by multi-collector ICP-MS. *Chem. Geol.* **188,** 65–83.

Criss R. E. (1999) Principles of Stable Isotope Distribution. Oxford University Press.

Dodson M. H. (1963) A theoretical study of the use of internal standards for precise isotopic analysis by the surface ionization technique: Part I. General first-order algebraic solutions. *J. Sci. Instrum.* **40,** 289–295.

Doucelance R. and Manhès G. (2001) Reevaluation of precise lead isotope measurements by thermal ionization mass spectrometry: Comparison with determinations by plasma source mass spectrometry. *Chem. Geol.* **176,** 361–377.

Eisele J., Abouchami W., Galer S.J.G., Hofmann A. W. (2002) The 320 kyr Pb isotope evolution of Mauna Kea lavas recorded in the HSDP-2 drill core. *Geochem. Geophys. Geosyst.* 4, doi:10.1029/2002GC000339.

Galer S. J. (1999) Optimal double and triple spiking for high precision lead isotopic measurement. *Chem. Geol.* **157,** 255–274.

Habfast K. (1998) Fractionation correction and multiple collectors in thermal ionization isotope ratio mass spectrometry. *Int. J. Mass Spec.* **176,** 133–148.

Hamelin B., Manhès G., Albarède F., and Allègre C. J. (1985) Precise lead isotope measurements by the double spike technique: A reconsideration. *Geochim. Cosmochim. Acta* **49,** 173–182.
Harper C. L. and Jacobsen S. B. (1992) Evidence from coupled 147Sm-143Nd and 146Sm-142Nd systematics for very early (4.5-Gyr) differentiation of the Earth's mantle. *Nature* **360,** 728–732.
Hart S. R. and Zindler A. (1989) Isotope fractionation laws: A test using calcium. *Int. J. Mass Spectr. Ion Proc.* **89,** 287–301.
Hofmann A. (1971) Fractionation corrections for mixed-isotope spikes of Sr, K, and Pb. *Earth Planet. Sci. Lett.* **10,** 397–402.
Johnson R. A. and Winchern D. W. (1992) Applied Multivariate Statistical Analysis. Prentice-Hall.
Kehm K., Hauri E. H., Alexander C.M.O.D., and Carlson R. W. (2003) High precision iron isotope measurements of meteoritic material by cold plasma ICP-MS. *Geochim. Cosmochim. Acta* **67,** 2879–2891.
Longerich H. P., Fryer B. J., and Strong D. F. (1987) Determination of lead isotope ratios by inductively coupled plasma-mass spectrometry (ICP-MS). *Spectrochim. Acta Part B* **42,** 39–48.
Ludwig K. R. (1997) Optimization of multicollector isotope-ratio measurement of strontium and neodymium. *Chem. Geol.* **135,** 325–334.
Luais B., Télouk P., and Albarède F. (1997) Precise and accurate neodymium isotopic measurements by plasma-source mass spectrometry. *Geochim. Cosmochim. Acta* **61,** 4847–4854.
Maréchal C., Télouk P., and Albarède F. (1999) Precise analysis of copper and zinc isotopic compositions by plasma-source mass spectrometry. *Chem. Geol.* **156,** 251–273.
Niu H. and Houk R. S. (1996) Fundamental aspects of ion extraction in inductively coupled plasma mass spectrometry. *Spectrochim. Acta Part B* **51,** 779–815.
Nyquist H. (1928) Thermal agitation of electric charge in conductors. *Phys. Rev.* **32,** 110–113.
Papanastassiou D. A., Sharma M., Ngo H. N., Wasserburg G. J., and Dymek R. F. (2003) No ^{142}Nd excess in the early archaean Isua gneiss IE 715–28. *Lunar Planet. Sci. Conf.* **34,** 1851(abstr.).
Powell R., Woodhead J., and Hergt J. (1998) Uncertainties on lead isotope analyses: Deconvolution in the double-spike method. *Chem. Geol.* **148,** 95–104.
Rehkämper M. and Mezger K. (2000) Investigation of matrix effects for Pb isotope ratio measurements by multiple collector ICP-MS: Verification and application of optimized analytical protocols. *J. Anal. At. Spectrom.* **15,** 1451–1460.
Rehkämper M. and Halliday A. N. (1998) Accuracy and long-term reproducibility of lead isotopic measurements by MC-ICP-MS using an external method for correction of mass discrimination. *Int. J. Mass Spectrom.* **181,** 123–133.
Russell W. A., Papanastassiou D. A., and Tombrello T. A. (1978) Ca isotope fractionation on the Earth and other solar system materials. *Geochim. Cosmochim. Acta* **42,** 1075–1090.
Sharma M., Papanastassiou D. A., Wasserburg G. J., and Dymek R. F. (1996) The issue of terrestrial record of ^{146}Sm. *Geochim. Cosmochim. Acta* **60,** 2037–2047.
Thirlwall M. (1991) Long-term reproducibility of multicollector Sr and Nd isotope ratio analysis. *Chem. Geol.* **94,** 85–104.
Thirlwall M. F. (2000) Interlaboratory and other errors in Pb isotope analyses investigated using a 207Pb-204Pb double spike. *Chem. Geol.* **163,** 299–1125.
Thirlwall M. F. (2002) Multicollector ICP-MS analysis of Pb isotopes using a 207Pb-204Pb double spike demonstrates up to 4000 ppm/amu systematic errors in Tl-normalization. *Chem. Geol.* **184,** 255–279.
Vance D. and Thirlwall M. F. (2002) An assessment of mass discrimination in MC-ICPMS using Nd isotopes. *Chem. Geol.* **185,** 227–240.
Walder A. J., Platzner I., and Freedman P. A. (1993) Isotope ratio measurement of lead, neodymium and neodymium-samarium mixtures, hafnium and hafnium-lutetium mixtures with a double focusing multiple collector inductively coupled plasma mass spectrometer. *J. Anal. At. Spectrom.* **8,** 19–23.
Wasserburg G. J., Jacobsen S. B., DePaolo D. J., McCulloch M. T., and Wen T. (1981) Precise determination of Sm/Nd ratios, Sm and Nd isotopic abundances in standard solutions. *Geochim. Cosmochim. Acta* **45,** 2311–2323.
Wendt I. and Haase G. (1998) Dynamic double collector measurement with cup efficiency factor determination. *Chem. Geol.* **146,** 99–110.
White W. M., Albarède F., and Télouk P. (2000) High-precision analysis of Pb isotopic ratios using multi-collector ICP-MS. *Chem. Geol.* **167,** 257–270.
Woodhead J. (2002) A simple method for obtaining highly accurate Pb isotope data by MC-ICP-MS. *J. Anal. At. Spectrom.* **17,** 1381–1385.

APPENDIX A: TABLE OF SYMBOLS

A: matrix of coefficients used for dynamic runs
$\mathcal{A}_k$: cup-dependent factor (efficiency) of Faraday cup k
f: mass bias factor for the generalized power law ($=q \ln h$)
$\mathcal{F}_i$: closure condition for the isotopic ratio N_i/N_{ref} in sample-spike mixtures (must be zero)
g: mass bias factor for the power law ($=e^{\delta}$)
h: mass bias factor for the generalized power law
M_i: atomic mass of nuclide i
N_i: number of nuclides i introduced into the mass spectrometer
n_i: number of nuclides i detected by the mass spectrometer
q: exponent of the atomic mass in the generalized power law (1 for the power law, 0 for the exponential law)
R^2: correlation coefficient of a regression line
R_i: true isotopic ratio N_i/N_{ref}
r_i: measured isotopic ratio n_i/n_{ref}
r_i^e: isotopic ratio n_i/n_{ref} corrected for an exponential bias
$s_{i/k}^{j/k}$: slope of the mass fractionation curve in a log-log plot
$\mathcal{T}_i^{\gamma}$: transmission for isotope i in cup γ
W: covariance matrix
x: vector of unknown parameters calculated from dynamic runs
y: vector of data used in dynamic runs
$\mathcal{H}$: mass bias factor for the power law of Kehm et al. (2003)
$\mathcal{Y}_i$: mass bias for isotope i
β: first-order mass bias factor for the exponential law ($=M_{\text{ref}}\delta$ and identical to f when $q = 0$)
γ: second-order mass bias factor for the exponential law
δ: mass bias factor for the linear law
μ_i: $\ln M_i/M_{\text{ref}}$
σ_A: thermal (Johnson) noise of the resistor (in A)
θ: interpolation parameter used for standard bracketing ($0 < \theta < 1$)
ε_i: deviation of the isotopic ratio from the reference value in part per 10,000 ($r_i/R_i - 1) \times 10{,}000$
$\Delta R/R$: Mass fractionation per atomic mass unit

APPENDIX B: ANALYTICAL CONDITIONS

The data presented here were acquired on the Fisons Instruments Plasma 54 of Lyon. The main features of this instrument are described by Walder et al. (1993). It is equipped with one axial collector and four lateral collectors on each side. The resistors (10^{11} Ω) are calibrated daily against a stable current source. The Glass Expansion nebulizer is fitted to microbore PFA tubing and is operated in free aspiration mode. Its uptake rate is about 50 microliters per minute. None of the results presented here were acquired with a desolvating nebulizer. A transmission of 30 V per ppm of Pb is routinely achieved. Off-line reduction of the data has now supplemented the original factory software. Samples are run in 0.05 N nitric acid. Concentrated (0.65 N) nitric acid and dilute hydrofluoric acid are used at the cleaning stage until the original signal declines to less than 10^{-14} A.